Cellular/Molecular

A Distinct Class of Slow (~0.2–2 Hz) Intrinsically Bursting Layer 5 Pyramidal Neurons Determines UP/DOWN State Dynamics in the Neocortex

Magor L. Lőrincz,[1,2] David Gunner,[3] Ying Bao,[2] William M. Connelly,[2] John T.R. Isaac,[3] Stuart W. Hughes,[3] and Vincenzo Crunelli[2]

[1]Research Group for Cellular and Network Neurophysiology of the Hungarian Academy of Sciences, Department of Physiology, Anatomy and Neuroscience, University of Szeged, 6726 Szeged, Hungary, [2]Neuroscience Division, School of Biosciences, Cardiff University, Cardiff CF10 3AX, United Kingdom, and [3]Lilly Research Laboratories, Surrey GU20 6PH, United Kingdom

During sleep and anesthesia, neocortical neurons exhibit rhythmic UP/DOWN membrane potential states. Although UP states are maintained by synaptic activity, the mechanisms that underlie the initiation and robust rhythmicity of UP states are unknown. Using a physiologically validated model of UP/DOWN state generation in mouse neocortical slices whereby the cholinergic tone present *in vivo* is reinstated, we show that the regular initiation of UP states is driven by an electrophysiologically distinct subset of morphologically identified layer 5 neurons, which exhibit intrinsic rhythmic low-frequency burst firing at ~0.2–2 Hz. This low-frequency bursting is resistant to block of glutamatergic and GABAergic transmission but is absent when slices are maintained in a low Ca^{2+} medium (an alternative, widely used model of cortical UP/DOWN states), thus explaining the lack of rhythmic UP states and abnormally prolonged DOWN states in this condition. We also characterized the activity of various other pyramidal and nonpyramidal neurons during UP/DOWN states and found that an electrophysiologically distinct subset of layer 5 regular spiking pyramidal neurons fires earlier during the onset of network oscillations compared with all other types of neurons recorded. This study, therefore, identifies an important role for cell-type-specific neuronal activity in driving neocortical UP states.

Key words: **acetylcholine; inhibition; muscarinic; rhythmic bursting; slow waves**

Introduction

In the absence of sensory input, the mammalian brain exhibits a wide array of structured, spontaneous activity. An example of this is the alternation of neocortical UP and DOWN states, which are periods of persistent, widespread network activity and collective neuronal disfacilitation, respectively (Crunelli and Hughes, 2010; Timofeev and Chauvette, 2011). Such UP and DOWN states are evident during non-REM sleep (Steriade et al., 2001; Timofeev et al., 2001; David et al., 2013) and under anesthesia where they occur rhythmically at ~0.2–1 Hz to form a slow oscillation (Steriade et al., 1993c; David et al., 2013). Up until now, synchronous UP and DOWN states have not been observed in neocortical slices maintained using a traditional recording medium (i.e., containing 2 mM Ca^{2+}) but have required a medium containing 1–1.2 mM Ca^{2+} that is purported to more closely reflect the *in vivo* ionic composition (Sanchez-Vives and McCormick, 2000; Cossart et al., 2003; Shu et al., 2003; see also Cunningham et al., 2006). Although this approach reproduces several properties of the *in vivo* UP/DOWN states, DOWN states are typically much more prolonged than *in vivo* (Sanchez-Vives and McCormick, 2000); and when applied in rodent neocortical slices, UP states tend to be sporadic and lack rhythmicity (e.g., Cossart et al., 2003; Fanselow and Connors, 2010). Thus, the mechanisms underlying the initiation and robust rhythmicity of UP states have remained elusive.

In anesthetized cats, UP and DOWN state duration is dramatically reduced by mAChR antagonists, suggesting a role for the cholinergic system in UP state generation (Steriade et al., 1993b). Although neurons in both brainstem cholinergic nuclei (Steriade et al., 1990) and basal forebrain (Szymusiak et al., 2000; Lee et al., 2004, 2005; Hassani et al., 2009) generally fire substantially less during sleep and drowsiness, their firing does not entirely cease. Indeed, although cortical ACh levels are diminished during slow-wave sleep, they nonetheless remain at significant levels (Marrosu

Received Aug. 26, 2014; revised Jan. 29, 2015; accepted Feb. 4, 2015.

Author contributions: M.L.L., J.T.R.I., S.W.H., and V.C. designed research; M.L.L., D.G., Y.B., W.M.C., and S.W.H. performed research; M.L.L., J.T.R.I., and S.W.H. analyzed data; M.L.L., S.W.H., and V.C. wrote the paper.

This work was supported by the Wellcome Trust 78403 and 91882 to V.C. and 78311 to S.W.H., Ely Lilly & Co. Lilly Research Award Program to V.C., Hungarian Brain Research Program KTIA_NAP_13-2-2014-0014 to M.L.L., Hungarian Scientific Research Fund OTKA NF 105083 to M.L.L., and Human Frontier Science Program fellowship LT001009/2010L to M.L.L. We thank Mr. Timothy Gould for technical assistance.

D.G., J.T.R.I., and S.W.H. were full-time employees of Eli Lilly & Co. when this research was conducted. The remaining authors declare no competing financial interests.

This article is freely available online through the *J Neurosci* Author Open Choice option.

Correspondence should be addressed to Dr. Magor L. Lőrincz, Research Group for Cellular and Network Neurophysiology of the Hungarian Academy of Sciences, Department of Physiology, Anatomy and Neuroscience, University of Szeged, Közép fasor 52, Szeged, 6726, Hungary. E-mail: mlorincz@bio.u-szeged.hu.

S.W. Hughes' current address: Vertex Pharmaceuticals (Europe) Ltd., 86-88 Jubilee Avenue, Milton Park, Abingdon, Oxfordshire OX14 4RW, United Kingdom.

DOI:10.1523/JNEUROSCI.3603-14.2015

et al., 1995; Vazquez and Baghdoyan, 2001). Furthermore, functional imaging in humans reveals a strong activation of brainstem regions that encompass cholinergic nuclei during slow waves (Dang-Vu et al., 2008).

Here we show that pharmacological reactivation of the cholinergic input in mouse neocortical slices brings about rhythmic UP and DOWN states with properties that are equivalent to those observed during the slow oscillation *in vivo*. We further demonstrate that UP states are driven by low-frequency (~0.2–2 Hz) rhythmic burst firing in a small subset of layer 5 neurons, which in these, but not in the remaining intrinsically bursting (IB) pyramidal neurons, is resistant to GABA and ionotropic glutamate receptor antagonists. Indeed, engagement of these putative "network driver" neurons by cholinergic activation is essential for bringing about the strong rhythmicity of UP states that is present *in vivo*. In contrast, a compromise of the "network driver" bursting in the low Ca^{2+} model explains the inability to consistently reproduce this key characteristic of the natural slow oscillation in previous *in vitro* studies using this model.

Materials and Methods

All procedures were performed in accordance with local ethical committee guidelines and the United Kingdom Animals (Scientific Procedure) Act, 1986. All efforts were made to minimize the suffering and number of animals used in each experiment.

Surgical procedures and in vivo *electrophysiology.* Male C57BL/6J mice (P30-P60, Harlan) were anesthetized with urethane (1.0 g/kg) and supplemented with ketamine and xylazine (20 and 2 mg/kg, respectively) to maintain anesthesia. Body temperature was maintained at constant levels using a heating plate (Supertech). After exposing the skull, a small hole was drilled above the target area at stereotaxic coordinates (anteroposterior: −3.1; lateral: 3.5–3.9 mm). Stainless steel screws (0.8 mm diameter) were placed into the skull over the cerebellum and the frontal cortex, which served as a ground and reference, respectively. Local field potentials (LFPs, filtered between 0.1 and 200 Hz) and extracellular single units (filtered between 0.5 and 5 kHz) were recorded using glass pipettes filled with ACSF (resistance: 500–600 kΩ for LFP, 4–6 MΩ for single units) connected to a Multiclamp 700B amplifier (Molecular Devices). Extracellular action potentials were recorded in loose-cell mode (seal resistance: 20–50 MΩ). Intracellular recordings were performed using glass electrodes filled with 1 M potassium acetate (resistance: 15–40 MΩ), and in some cases 2% biocytin or neurobiotin, and connected to an Axoclamp-2A amplifier (Molecular Devices) operating in bridge mode. Voltage records were digitally acquired and processed using pClamp 9 (Molecular Devices). All *in vivo* intracellular and extracellular recordings were obtained from the primary auditory cortex (Crunelli et al., 2012). Scopolamine (1 mM) was added to the ACSF present in the recording chamber (constructed from dental acrylic cement) that was fixed to the mouse skull. At the end of the experiments, the animals were given a lethal dose of urethane.

In vitro *slice preparation and maintenance.* Male C57BL/6J mice (P21-P60, Harlan) were deeply anesthetized with isoflurane, decapitated, and the brain quickly removed into continuously oxygenated (95% O_2/5% CO_2) 4°C cutting solution containing the following (in mM): 60 sucrose, 85 NaCl, 2.5 KCl, 1.25 NaH_2PO_4, 2 $MgCl_2$, 25 $NaHCO_3$, 1 $CaCl_2$, 25 $NaHCO_3$, 10 glucose, 0.045 indomethacin, and 3 kynurenic acid. Coronal slices (400 μm thick) containing the auditory, somatosensory, visual, temporal association, or medial prefrontal cortex were cut on a vibrotome (Leica). Slices were allowed to recover for 60 min at room temperature. For recording, slices were perfused in an interface chamber with a warmed (35 ± 1°C) continuously oxygenated (95% O_2, 5% CO_2) ACSF containing the following (in mM): 134 NaCl, 2 KCl, 1.25 KH_2PO_4, 1 $MgSO_4$, 2 $CaCl_2$, 26 $NaHCO_3$, and 10 glucose. Drugs were dissolved directly in either ACSF or in DMSO, in which case the concentration of DMSO did not exceed 0.1% v/v. The modified ACSF contained (mM) the following: 125 NaCl, 3.5 KCl, 1.25 NaH_2PO_4, 1 $MgCl_2$, 1.0–1.2 $CaCl_2$, 25 $NaHCO_3$, and 10 glucose.

In vitro *electrophysiology.* Extracellular recordings were performed using glass pipettes filled with ACSF (resistance: 1–5 MΩ) connected to a Neurolog 104 differential amplifier (Digitimer). Field and unit activities were simultaneously recorded through the same electrode by bandpass filtering at 0–200 Hz and 0.2–5 kHz, respectively. Multisite extracellular recordings were performed with linear arrays (FHC) connected to a multichannel differential amplifier (Plexon or Neuralynx). In all cases, the interelectrode distance was 190 μm. Independently mounted intracellular recordings, using the current-clamp technique, were performed with standard-wall glass microelectrodes filled with 1 M potassium acetate (resistance: 80–120 MΩ), and in some cases 2% biocytin or neurobiotin, and connected to an Axoclamp-2A amplifier (Molecular Devices) operating in bridge mode. Voltage and current records were digitally acquired and processed using pClamp 9 (Molecular Devices). Unless explicitly stated otherwise, all *in vitro* recordings were obtained from slices of the primary auditory cortex.

Data analysis. UP states from the LFP signal were detected from the high pass filtered and trace (Mukovski et al., 2007), and a minimum of 100 cycles for each recorded neuron were used to perform statistical analysis. Phase values of neuronal firing relative to the EEG or LFP, expressed as the angle of the mean vector (μ), and strength of phase coupling, expressed as the normalized mean vector length (r), were computed with circular statistical methods using Oriana 2.0 software (Kovach Computing Services). The range of r is 0 to1, with a value of 1 representing perfect phase coupling, whereas when events are random $r \rightarrow 0$. Absolute spike times were established using a straightforward visually determined threshold approach. To construct a spike-timing histogram, the times of >500 consecutive spikes were determined relative to the nearest negative peaks of the LFO using custom-written transform routines in SigmaPlot 9 (Systat). These times were subsequently assigned a given phase between these peaks (i.e., between 0° and 360°), binned at 20°. The values in each bin were then divided by the total number of oscillation cycles to give a value in units of spikes per bin. For clarity, and to afford a sense of rhythmicity, these data were plotted over two full cycles of the oscillation (−360° to 360°) to produce the final plot (Lőrincz et al., 2009). For measuring the membrane potential of UP and DOWN states, we generated a membrane potential distribution plot and used the peaks (or peak for nonbimodal UP/DOWN states) from these plots to produce these values. All auto-correlation, cross-correlation, and power spectra plots were produced with OriginPro 8.0 (OriginLab). All quantitative data are expressed as mean ± SEM, and statistical significance was assessed using Student's *t* test.

Histology. Intracellularly recorded cells were labeled by applying depolarizing current steps (0.3–0.6 nA, 500 ms, 1 s duty cycle) for 10 min through the bridge circuitry. Slices were fixed in 4% PFA overnight. Cells were visualized using the avidin-biotin-HRP reaction as previously described (Lőrincz et al., 2009) and were reconstructed using Neurolucida (MicroBrightField Europe).

Sources of drugs. DL-APV (NMDA receptor antagonist), CNQX (AMPA/kainate receptor antagonist), CGP 54626 hydrochloride ($GABA_B$ antagonist) 1,1-dimethyl-4-diphenylacetoxypiperidinium iodide (4-DAMP) (M3 receptor antagonist), 8-methyl-8azabicyclo-3-*endo*[3,2,1]oct-3-yl-1,4-dihydro-2-oxo-3(2*H*)-quinazolinecarboxylic acid ester hydrochloride (DAU-5884) (M3 receptor antagonist), 2,3-dihydroxy-6-nitro-7-sulfamoyl-benzo[f]quinoxaline-2,3-dione (NBQX) (AMPA/kainate receptor antagonist), 6-imino-3-(4-methoxyphenyl)-1(6*H*)-pyridazinebutanoic acid hydrobromide (SR95531, gabazine) ($GABA_A$ receptor antagonist), and 4,9-dihydro-3-methyl-4-[(4-methyl-1-piperazinyl)acetyl]-10*H*-thieno[3,4-b][1,5]benzodiazepin-10-one dihydrochloride (telenzepine) (M1 receptor antagonist) were from Tocris Cookson; carbamylcholine chloride (carbachol, CCH) (nonselective cholinergic agonist) and 5,11-dihydro-11-([4-methyl-piperazin]acetyl)-6H-pyriso(2,3-b) (1,4) benzodiazepine-6-one (pirenzipine) (M1/M3 receptor antagonist) were obtained from Sigma.

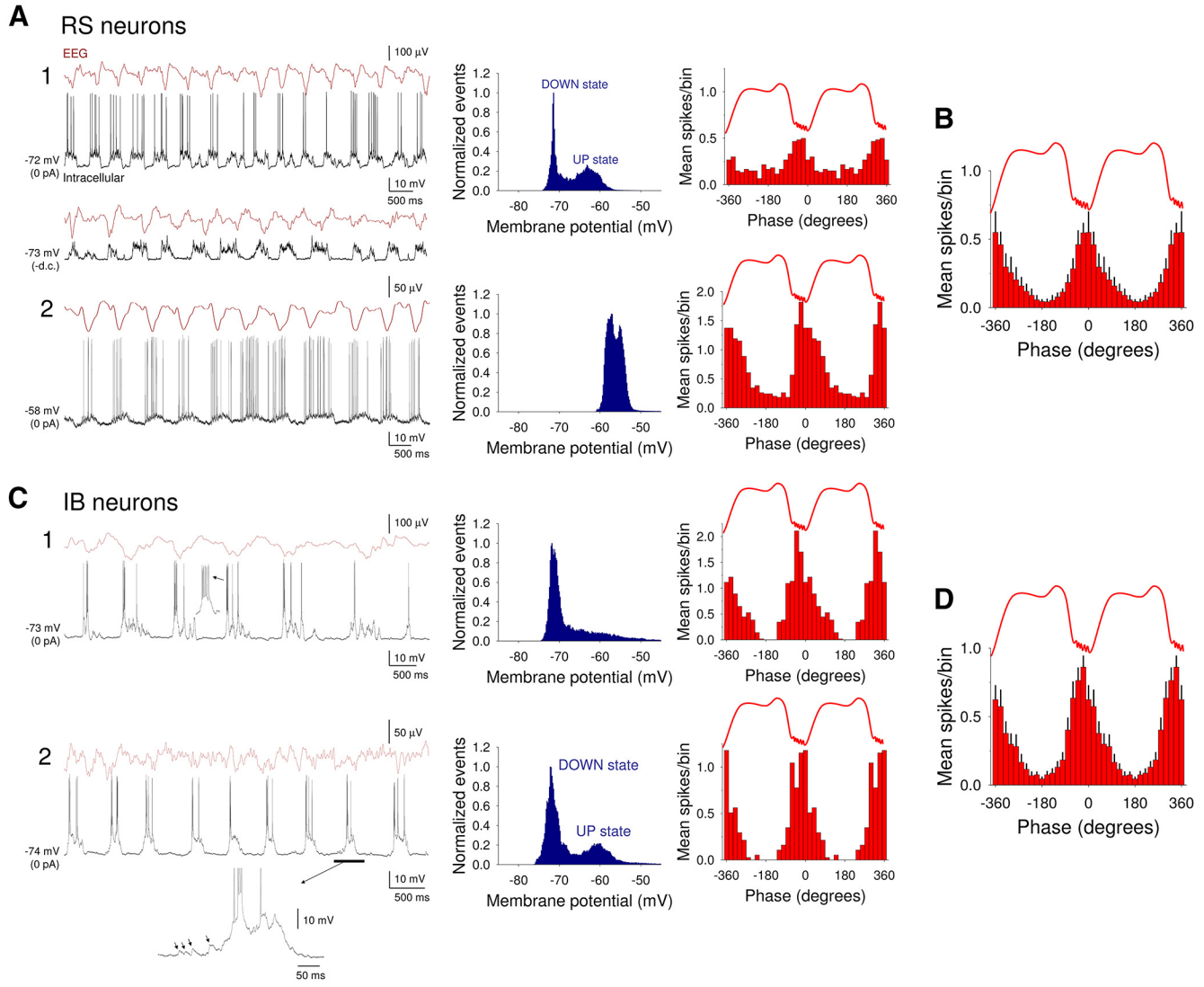

Figure 1. Recordings of the slow (<1 Hz) oscillation and corresponding UP and DOWN states from layer 5 of the auditory cortex in the anesthetized mouse. ***A***, Simultaneous EEG and intracellular recordings from two RS neurons showing representative examples of UP and DOWN states from neurons where membrane potential is distributed bimodally (***A*** $_1$) and nonbimodally (***A*** $_2$). The corresponding membrane potential distributions are shown to the immediate right (blue plots), whereas the related spike timing histograms (red bars) are plotted on the far right. Hyperpolarization of the neuron in ***A*** $_1$ to prevent action potential firing (bottom trace, −d.c.) reveals barrages of synaptic activity during UP states. The UP states in the RS neuron depicted in ***A*** $_2$ emerge from a relatively depolarized membrane potential baseline. ***B***, Average spike timing histogram (mean ± SEM) computed from 12 RS neurons. ***C***, Simultaneous EEG and intracellular recordings from two different IB neurons. UP states arise consistently from a hyperpolarized membrane potential baseline and always commence with a burst of action potentials. The corresponding membrane potential distributions are shown to the immediate right (blue plots), whereas the related spike timing histograms (red bars) are plotted on the far right. ***D***, Average spike timing histogram computed from 12 IB neurons.

Results

UP and DOWN states in neocortical neurons of anesthetized mice

Intracellular recordings from neocortical neurons in layer 5 obtained under anesthesia exhibited prominent, rhythmic UP/DOWN states (0.85 ± 0.04 Hz; $n = 20$) (Fig. 1*A*,*C*). UP states in neocortical neurons were characterized by brief barrages of synaptic activity that were accompanied by prominent action potential firing (Fig. 1*A*,*C*). During the course of our experiments, we encountered both regular spiking (RS) ($n = 15$) (Fig. 1*A*) and IB ($n = 19$) (Fig. 1*C*) neocortical neurons. In the majority of RS cells ($n = 11$ of 15; 73%), UP states arose from a relatively hyperpolarized baseline and led to clear membrane potential bimodality (DOWN state: −73.7 ± 2.5 mV; UP state: −61.2 ± 1.4 mV; $n = 8$) (Fig. 1A_1). In other RS cells, UP states could also emerge from a more depolarized baseline leading to an undulating appearance and a lack of membrane potential bimodality ($n = 3$ of 15; 20%) (Fig. 1A_2), as seen previously in cats (Steriade et al., 1993a). Indeed, in some RS cells, UP states essentially appeared on top of a baseline (i.e., DOWN state) that already exhibited some tonic action potential output (Fig. 1A_2). Such a pattern of activity is not due to damage done to the cell by intracellular impalement because it has also been observed in single-unit extracellular recordings (Crunelli et al., 2012). When RS cells were considered together, action potential output occurred primarily close to the negative peaks of the LFP ($\mu = -4.3 \pm 6.6°$; $n = 15$), with cells showing a normalized vector length (r) of 0.61 ± 0.09 ($n = 15$) (Fig. 1*B*).

In contrast to RS cells, UP states in IB cells always emerged from a relatively hyperpolarized baseline (Fig. 1*C*). As such, action potential activity was rarely observed in these cells during the DOWN state, and they were typically associated with membrane

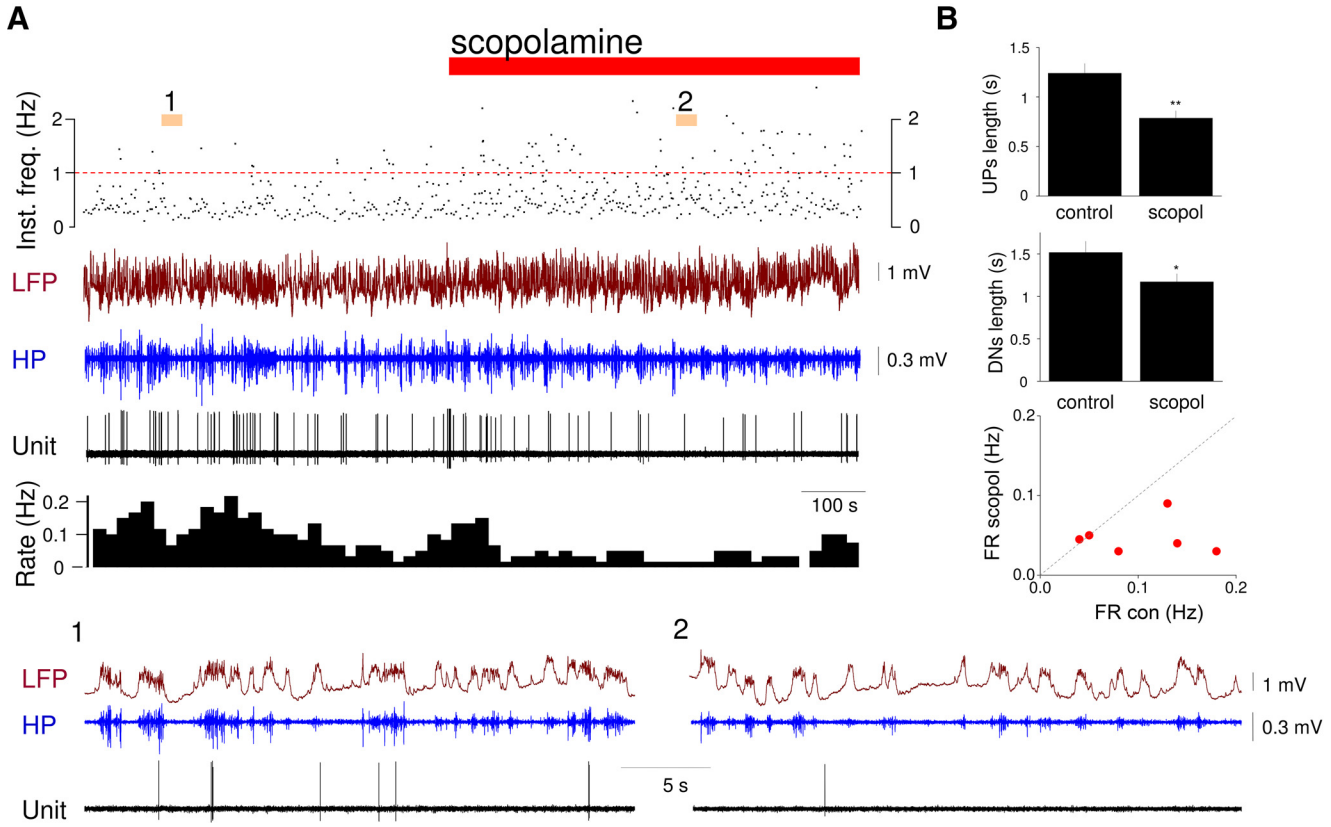

Figure 2. Neocortical UP states in anesthetized mice are dependent on mAChRs. ***A***, Representative simultaneous recordings of the layer 2/3 LFP and single-unit activity in the auditory cortex of an anesthetized mouse before and after local administration of the nonselective mAChR antagonist, scopolamine (red bar, 1 mM applied in the chamber fixed to the skull; see Materials and Methods). Top plot, The instantaneous frequency (Inst. freq.) of UP states detected from the LFP signal. Below the LFP, the high pass filtered (HP, 20–100 Hz) signal is plotted. The corresponding firing rate histogram (10 s bin size) is shown below the unit recording. ***A*$_1$, ***A*$_2$, Plotted below on a faster time base. ***B***, UP state (top) and DOWN state (middle) durations for control and scopolamine (scopol) conditions in anesthetized mice (mean ± SEM; $n = 6$). *$p < 0.05$. **$p < 0.001$. Scatter plot (bottom) comparing mean firing rates (FR) before (con) and after scopolamine (scopol) administration.

potential bimodality (DOWN state: −74.3 ± 2.2 mV; UP state: −60.1 ± 1.9 mV; $n = 19$) (e.g., Fig. 1C_1). A robust burst was almost always present at the beginning of an UP state in IB neurons (Fig. 1C_1,C_2, insets) (Steriade et al., 1993a). In these cells, UP states were also often preceded by a buildup of spontaneous EPSPs (Fig. 1C_2, inset, arrows). Firing in IB cells was found to occur slightly earlier than in RS cells ($\mu = -15.8 \pm 6.9°$; $n = 6$, $p = 0.03$) (Fig. 1*D*). There was no difference in the strength of phase coupling for IB cells compared with RS cells ($r = 0.58 \pm 0.07$; $n = 19$; $p > 0.5$).

Neocortical UP states in anesthetized mice are dependent on mAChRs

In anesthetized cats, systemic administration of the mAchR antagonist scopolamine leads to a substantial reduction in the duration of both UP states and DOWN states, indicating an important role for mAChRs in controlling UP states in this species (Steriade et al., 1993b). To test whether mAChRs also influence neocortical UP states in mice, we locally administered scopolamine to the auditory cortex of anesthetized animals (1 mM; see Materials and Methods) while monitoring UP states using extracellular LFP and single-unit recordings (Fig. 2). The effects of local scopolamine administration were clearly evident in the LFP where they were reflected as a reduction in the duration of both UP (control: 1.2 ± 0.1 s; scopolamine: 0.7 ± 0.1 s; $n = 5$; $p < 0.001$) and DOWN states (control: 1.5 ± 0.1 s, scopolamine: 1.1 ± 0.1 s; $n = 5$; $p < 0.05$) (Fig. 2). The associated action potential output during UP states also decreased (control: 0.1 ± 0.05 Hz; scopolamine: 0.04 ± 0.02 Hz; $n = 6$ neurons; $p < 0.001$).

Activation of cholinergic receptors brings about a slow (<1 Hz) oscillation and associated rhythmic UP/DOWN states in mouse neocortical slices

Given that neocortical UP states in anesthetized mice are suppressed by scopolamine administration, we examined the effects of the nonselective AChR agonist carbachol (CCH, 30–50 μM) on network excitability in slices of the primary auditory cortex from adult mice. When assessed with extracellular multielectrode array recordings in control conditions, there was a lack of spontaneous activity in all slices ($n = 140$ slices) (Fig. 3*A–C*). Correspondingly, intracellular recordings from neocortical neurons revealed a hyperpolarized membrane potential (<−60 mV), a lack of spontaneous action potential firing, and only sporadic, uncoordinated synaptic activity (Fig. 3*C*). Immediately following CCH application, extracellular recordings revealed the appearance of LFP oscillations at ~2–4 Hz in layer 5 (Fig. 3A_1). Over the subsequent course of a few minutes, these LFP oscillations increased in amplitude, slowed to ~0.6 Hz (0.66 ± 0.17 Hz; $n = 10$), and became evident in other cortical layers (Fig. 3A_2).

When assessed with extracellular recordings, CCH application was associated with a rapid and pronounced increase in spontaneous action potential firing that almost exclusively consisted of single spike or tonic activity (9.77 ± 6.77 Hz, $n = 32$ neurons of 150, 21%) that was present even before the emergence of LFP oscillations (Fig. 3*B*, top right). Neurons that generated

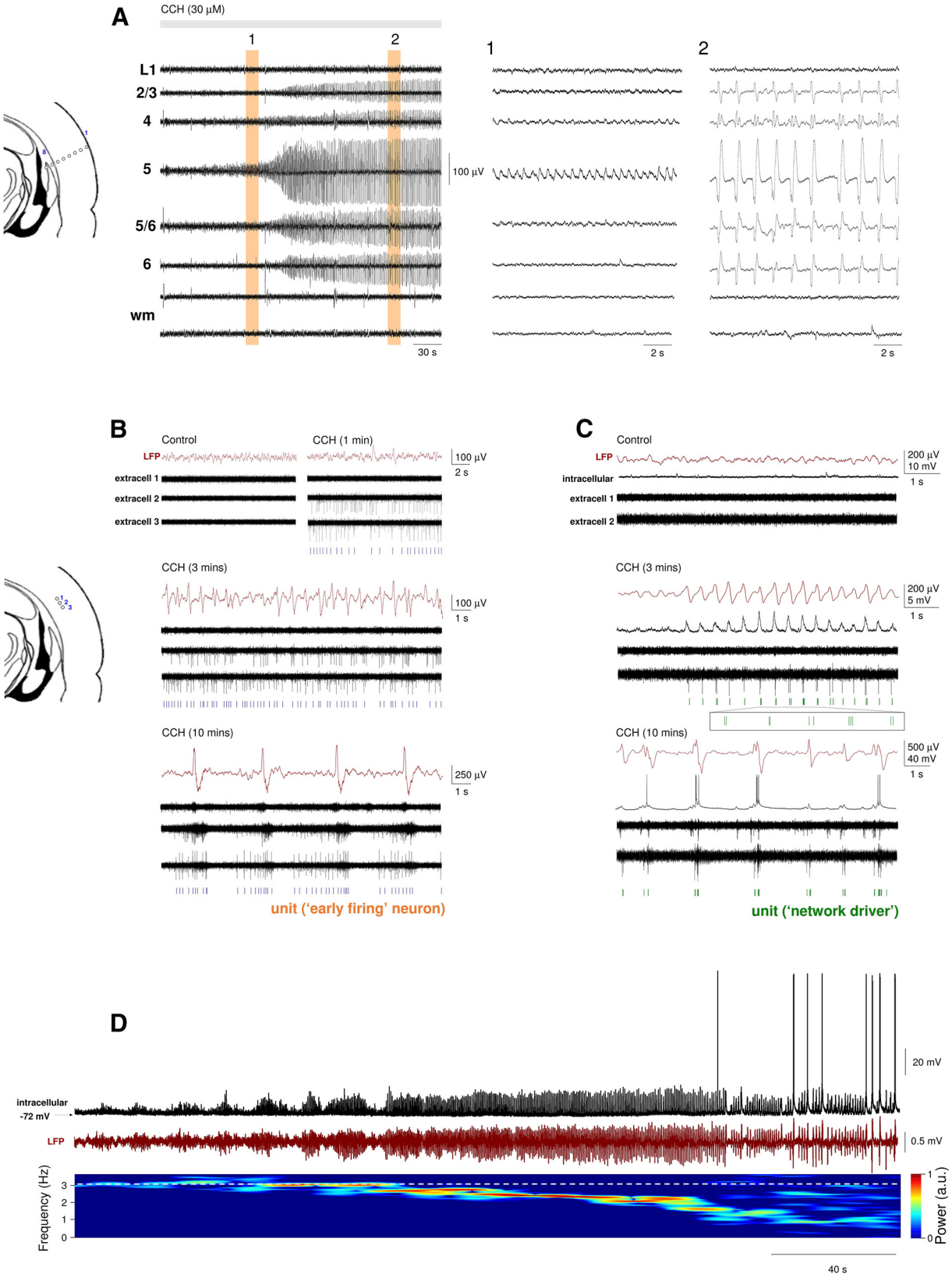

Figure 3. Reinstating the cholinergic drive brings about a prominent slow (<1 Hz) oscillation and associated UP and DOWN states in slices of the mouse auditory cortex. ***A***, Multisite LFP recording from different layers of the auditory cortex using an 8 electrode linear array (arrangement depicted on the far left). Application of the nonselective cholinergic receptor agonist CCH (30 μM) initially brings about oscillatory activity at ~2 Hz in layer 5 (A_1), which progressively slows down to ~0.6 Hz and spreads to other cortical layers (A_2). wm, White matter. ***B***, Multisite extracellular recordings obtained with an 8 electrode linear array placed approximately across layer 5 (arrangement depicted on the far left). CCH application causes the rapid appearance of continuous firing (top right, *extracell 2* and *extracell 3*, "early firing" cells), which is not initially phase-locked to oscillations in the LFP recorded in the same layer (middle traces) but later becomes fully entrained to network activity once the slow oscillation is fully developed (bottom traces). ***C***, Multisite extracellular recordings obtained with an 8 electrode linear array placed in the (*Figure legend continues.*)

this firing were termed "early firing" cells. Interestingly, upon the emergence of LFP oscillations at 2–4 Hz (Fig. 3*B*, middle), activity in "early firing" cells was usually not immediately entrained to the LFP fluctuations (Fig. 3*B*, middle) and often only became fully engaged in network activity later on when slow (<1 Hz) oscillations dominated the LFP (Fig. 3*B*, bottom). In contrast to "early firing" cells, in a separate group of neurons, a distinct type of firing consisting primarily of brief bursts was initiated simultaneously with the onset of LFP oscillations ($n = 12$ neurons of 150, 8%), with this firing being robustly synchronized with the negative LFP peaks (Fig. 3*C*, middle). These neurons were termed putative "network drivers." Apart from "early firing" cells and "network drivers," all other cells ($n = 106$) commenced firing only after oscillation onset had occurred, at which point it was immediately synchronized with the LFP (e.g., Fig. 3*C*, intracellular). For such cases, simultaneous intracellular recordings revealed the appearance of rhythmic EPSPs phase-locked to 2–4 Hz oscillations, followed by firing and full-blown UP states when slow (<1 Hz) oscillations were fully developed (Fig. 3*C*, intracellular). The transformation of 2–4 Hz oscillation to slow (<1 Hz) oscillations was gradual (Fig. 3*D*).

Importantly, CCH-elicited network oscillations and correlated cellular firing, observed in the auditory cortex, could also be recorded in medial prefrontal, somatosensory, visual, and temporal association cortex (data not illustrated). In agreement with our *in vivo* results, CCH-elicited network oscillations could be blocked by the nonselective mAchR antagonist scopolamine (5 μM, $n = 5$), the M1 antagonists pirenzipine (1 μM, $n = 6$), telenzepine (2 μM, $n = 5$), and by the M3 receptor-preferring antagonists DAU-5884 (2 μM, $n = 5$) and 4-DAMP (1 μM, $n = 4$) (data not illustrated) indicating a reliance of UP states on both types of muscarinic receptors. Thus, pharmacologically reinstating the cholinergic drive with CCH is sufficient to bring about slow network oscillations and rhythmic UP/DOWN state dynamics in slices of the mouse neocortex.

Further analysis of network activity using extracellular multielectrode recordings, obtained with 8, 16, or 32 channel arrays, revealed that CCH-induced UP states showed widespread synchronization across the cortical slice being apparent at all recording sites (Figs. 3*A* and 4). Overall, the most pronounced activity was recorded in deep layers (i.e., layer 5 and 6; Fig. 4*A*, top), with current source density analysis revealing that the initiation of each oscillatory cycle was associated with a prominent current sink around layer 5 (Fig. 4*A*, bottom left). To estimate the relative timing of synchronized activity in regional neuronal populations, we examined cross-correlograms of the LFP recorded in different layers. In accordance with other *in vivo* and *in vitro* studies (Sanchez-Vives and McCormick, 2000; Sakata and Harris, 2009; Beltramo et al., 2013; Hughes and Crunelli, 2013), these revealed that, in the majority of cases, the oscillation starts in layer 5 and then spreads to layer 6 before propagating to more superficial layers (Fig. 4*A*, bottom right).

The propagation of oscillatory activity from layer 5 to layer 6 and subsequently to superficial layers observed for LFPs (Fig. 4*A*, bottom right) also held true when the timing of multiple single-unit extracellular action potentials recorded from different cortical layers was compared using multielectrode arrays: in the majority of cases ($n = 14$ of 17), layer 5 neurons discharged before neurons in deeper and more superficial layers (Fig. 4*A*, bar graph). However, in a few cases ($n = 3$ of 17), the layer of initiation could alternate in a seemingly random manner between layer 5 and layer 2/3 (Fig. 4*B*). Interestingly, in those cases where UP states appeared to commence in layer 2/3, the duration of UP states in this layer was significantly longer than when UP states commenced in layer 5 (524 ± 96 ms vs 310 ± 28 ms; $n = 30$ UP states from 3 slices; $p < 0.05$) (Fig. 4*C*, top right plot). Overall, the mean firing rate during UP states was significantly higher in layer 5 than in layer 2/3 (layer 5: 22.6 ± 4.9 Hz; layer 2/3 12.3 ± 3.3 Hz, $n = 50$ UP states from 5 slices; $p < 0.001$) (Fig. 4*C*, bottom plots).

As is the case *in vivo* (Steriade et al., 1996; Hasenstaub et al., 2005; Mukovski et al., 2007; Ruiz-Mejias et al., 2011; Crunelli et al., 2012), UP states induced by CCH in neocortical slices were associated with prominent high-frequency (~20–100 Hz) oscillations in the LFP (Fig. 5*A*). These oscillations occurred at a mean frequency of 52.4 ± 1.5 Hz ($n = 57$) (Fig. 5*B*) and were tightly synchronized within local neocortical areas (mean time lag in cross-correlation over 190 μm: 0.45 ± 0.08 ms; $n = 20$ pairs of recordings from 4 slices) (Fig. 5*C*). Interestingly, when assessed with linear electrode arrays placed approximately parallel to the cortical layers, epochs of high-frequency oscillations tended to randomly switch between different directions of propagation (Fig. 5*C*, top and middle traces) or appear to not propagate at all (Fig. 5*C*, bottom traces). This was not related to the propagation of the slow oscillation (i.e., underlying UP states), which typically remained relatively constant in this orientation (Fig. 5*C*, red dots, *D*). In addition, regardless of the manner in which epochs appeared to propagate, the tight local synchrony of high-frequency oscillations, the duration of oscillation epochs and the mean frequency within epochs remained unchanged (Fig. 5*C*, far right column, *D*). Simultaneous intracellular and extracellular recordings (Fig. 5*E*) showed that high-frequency oscillations in the LFP were clearly correlated with synaptic fluctuations (as shown for an RS cell in Fig. 5*E1*,*E2*) and therefore also action potential output in individual pyramidal neurons (Fig. 5*E*, bottom right). All types of cells recorded in this study (i.e., RS, IB, and nonpyramidal neurons) showed evidence of phase-coupling of their spikes to high-frequency oscillations (Fig. 5*F*).

In addition to layer 5 IB and RS pyramidal neurons, we also obtained intracellular recordings in neocortical slices from a variety of nonpyramidal neurons in infragranular cortical layers (i.e., 5/6; Fig. 6). Recordings of nonpyramidal neurons were subdivided into three groups: FS (fast-spiking) neurons, LTS (low threshold-spiking) neurons, and UC (unclassified) cells, some of which had late-spiking characteristics but did not consistently possess the morphology that identified them as a well-characterized neocortical cell class (Fig. 6*C*, top). All FS neurons were tightly phase-coupled to the LFP ($r = 0.58 \pm 0.09$; $n = 4$) with action potential output being maximal before the negative LFP peak ($\mu = -23.4 \pm 29.4°$; $n = 4$) (Fig. 6*A*). In contrast, LTS neurons showed much weaker phase-coupling to the LFP ($r = 0.26 \pm 0.06$; $n = 9$; $p < 0.05$) and exhibited no obvious peak in firing relative to the LFP (Fig. 6*B*). Phase-coupling for UC neurons was not significantly different from FS neurons ($r = 0.76 \pm$

←

(*Figure legend continued.*) same orientation as in ***B*** with an additional intracellular recording simultaneously obtained from layer 5. The emergence of network oscillations is immediately accompanied by synchronous burst firing in one of the extracellular recordings (middle traces, *extracell 2*, "network driver" cell). In contrast, in the intracellularly recorded RS neuron, the rhythmic EPSPs are initially correlated with LFO network oscillations and eventually become full-blown UP states once slow (<1 Hz) oscillations are fully developed. ***D***, LFP and intracellular recording from layer 5 during the onset of CCH (30 μM) induced network oscillations. The increase in LFP amplitude and correlated synaptic potentials eventually lead to action potential output. The gradual decrease in the dominant LFP frequency can be observed on the spectrogram below.

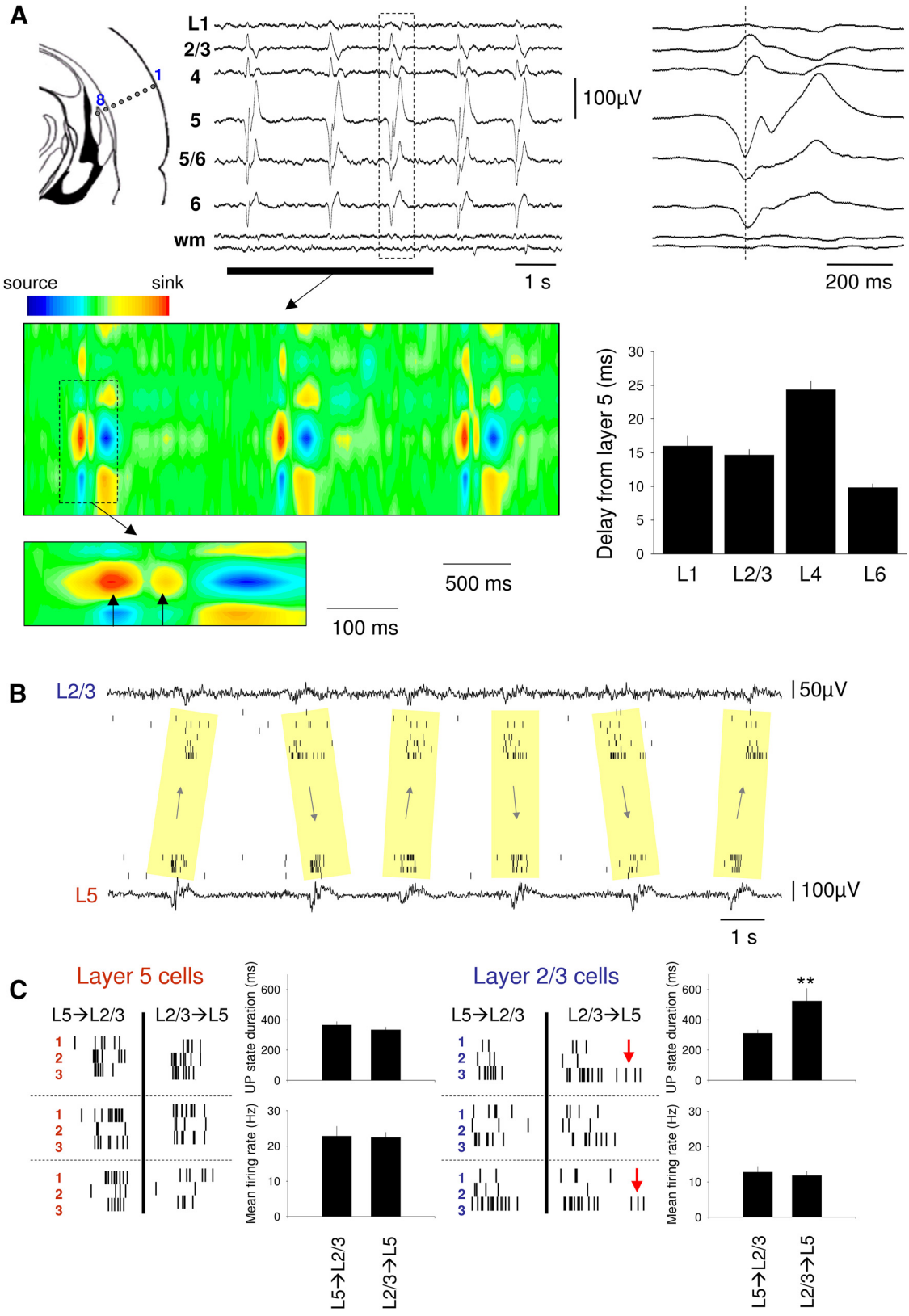

Figure 4. Layer-specific features of the CCH-induced slow oscillation in slices of the mouse auditory cortex. ***A***, Multisite recording of the LFP from different layers of the auditory cortex using an 8 electrode linear array (arrangement depicted on the far left) in the presence of 30 μM CCH. The most pronounced oscillatory activity is clearly evident in deep (infragranular) cortical layers. One cycle of the oscillation (boxed section) is expanded on the far right and shows a clear reversal of the oscillation sign between infragranular and supragranular layers. The corresponding current source density of the underlined section is shown below as indicated. Each cycle of the oscillation is initiated by a prominent current sink in layer 5. Expansion of the boxed section of the current source density further below shows that this initial current sink is closely followed by another, less prominent one, which is indicative of recurrent excitation (compare Fig. 2*A*). Bottom right, The plot shows the quantified delay of activity in each layer compared with layer 5 (L6 significantly different from L2, L3 and L4, and L4 from L2 and L3, all $p < 0.01$). ***B***, Simultaneous LFP and multiple single-unit recordings from L2/3 and L5 from one of the cases where activity could commence either in supragranular or infragranular layers. This could alternate between different (*Figure legend continues.*)

0.11; $n = 5$; $p = 0.23$) but was significantly stronger than for LTS cells ($p < 0.005$) (Fig. 6*C*). Peak firing in UC cells occurred close to the negative LFP peak ($\mu = -17.4 \pm 29.3°$; $n = 5$) (Fig. 6*C*). Finally, in all nonpyramidal neurons recorded ($n = 16$; see Fig. 6), development of UP states and engagement in network oscillations occurred via the gradual increase in the amplitude of LFP-related postsynaptic potentials (data not illustrated).

Putative "network drivers" are a subset of layer 5 IB pyramidal neurons

To understand the mechanisms that lead to network oscillations and UP/DOWN states in neocortical slices, we obtained intracellular recordings of neocortical neurons, both during the onset of LFP oscillations and subsequently for a prolonged period when the slow (<1 Hz) oscillation has been fully established. Of our total sample of 86 intracellularly recorded neurons, 6 (i.e., 7%) were identified as putative "network driver" neurons (i.e., cells where burst firing commenced simultaneously), and in synchrony, with 2–4 Hz LFP oscillations (delay from LFP onset: 3.3 ± 1.8 s, $n = 6$) (Figs. 3*C* and 7*A*,*C*; see 12*D*). All "network driver" cells were layer 5 IB pyramidal neurons that in control conditions were able to exhibit intrinsic rhythmic bursting at ~0.2–2 Hz in response to positive d.c. current injection (Fig. 8*A*). Following application of CCH, these cells were depolarized (control: −76.8 ± 4.4 mV; CCH: −62.4 ± 3.5 mV; $n = 6$) and became able to generate these rhythmic bursts spontaneously, with bursting occurring immediately in close association with negative peaks in the LFP (Fig. 8*A*, right; see also Fig. 12*D*). After a short period (~30–60 s), these bursts were occasionally closely followed by an additional depolarization indicative of recurrent excitation (Fig. 7*A*, middle, arrows). Over the course of the subsequent few minutes, these additional depolarizations became increasingly common and prolonged, eventually developing into full-blown, bimodal UP states that were present on every cycle of the oscillation (DOWN state: −70.4 ± 0.7 mV; UP state: −52.4 ± 1.5 mV; $n = 6$) (Fig. 7*A*, right). "Network driver" neurons never changed category over the entire duration of the recordings.

Whereas all "network driver" cells were found to be layer 5 IB pyramidal cells, not all layer 5 IB pyramidal neurons commenced firing simultaneously with the onset of LFP oscillations, with some of these cells being recruited to fire only after (delay from LFP onset: 30.5 ± 10.4 s; Fig. 7*C*), the LFP oscillation had been initiated (8 of 86; 9%; Fig. 7*D*). Following a similar CCH-induced depolarization to that which occurs in "network driver" cells (control: −73.6 ± 2.7 mV; CCH: −67.7 ± 3.5 mV; $n = 8$), this recruitment occurred via the gradual emergence, and increase in the amplitude, of LFP-associated rhythmic EPSP complexes in these cells (Fig. 7*D*, left). However, once fully recruited into slow (<1 Hz) oscillations, UP states in these neurons displayed a similar form to "network driver" cells in that they were always initiated by a burst of action potentials (Fig. 7*D*, middle and right) and were typically associated with membrane potential bimodality (DOWN state: −69.9 ± 0.7 mV; UP state: −53.3 ± 1.1 mV; $n = 8$) (Fig. 7*B*,*E*). As such, there was no difference in the timing of action potential output relative to the LFP between "network driver" and non-"network driver" IB cells with firing occurring at a mean phase (μ) of −18.9 ± 7.3° ($n = 14$; 6 "network driver" neurons, 8 conventional IB cells) and showing a normalized vector length (r) of 0.91 ± 0.02 ($n = 14$) (Fig. 7*F*). An additional shared feature was the common presence of a buildup of EPSPs just before the generation of an UP state (Fig. 7*D*, middle and right) as is also present *in vivo* (Fig. 1*C*, bottom). We also observed no obvious differences in cell morphology between "network driver" cells and other IB neurons, with all cells showing morphology typical of layer 5 IB pyramidal cells reported previously (Chagnac-Amitai et al., 1990; Franceschetti et al., 1993), comprising a relatively thick apical dendrite, prominent apical dendritic tuft, and an extensively arborizing axon in deep cortical layers (Fig. 8*A*,*B*, right).

Thus, the most apparent difference between "network driver" cells and the remainder of layer 5 IB pyramidal neurons is that the former respond more readily to CCH with low-frequency (~0.2–2 Hz) rhythmic bursting. Importantly, this is due solely to a direct depolarization of these neurons rather than a modulation of their intrinsic properties because, in the absence of CCH, intrinsic low-frequency rhythmic bursting could be readily brought about by injecting a small amount of steady depolarizing current (Fig. 8*A*), with larger amounts of current leading to single spike activity (compare Wang and McCormick, 1993; Schwindt et al., 1997). In contrast, in IB cells that are not "network driver" cells, burst firing occurred at notably higher frequencies than in "network driver" cells (Fig. 8*B*,*C*) (compare Schwindt et al., 1997).

"Early firing" cells are a subset of layer 5 RS pyramidal neurons

We next turned our attention to "early firing" cells: neurons in which preestablished (delay of LFP onset from start of firing: 123.45 ± 19.96 s, $n = 11$) (Figs. 3*B* and 9*A*,*C*) spontaneous single spike firing is gradually entrained to network activity. Overall, 26% (i.e., 22 of 86) of intracellularly recorded neurons were of this type. All "early firing" cells were layer 5 RS pyramidal neurons (Fig. 9*A*, left). Following application of CCH, these cells were rapidly and strongly depolarized (control: −66.6 ± 5.3 mV; CCH: −52.5 ± 3.1 mV; $n = 11$), leading to continuous firing (9.7 ± 2.29 Hz; $n = 11$) (Fig. 9*A*, left). As stated above, the subsequent onset of LFP oscillations was not always immediately associated with an appreciable change in this firing. However, as the slow (<1 Hz) oscillation in the LFP developed, the firing of these neurons became entrained to network oscillations (Fig. 9*A*, middle and right). On each oscillation cycle, this was characterized by a progressive buildup of firing followed by a pronounced hyperpolarization that occurred after the negative LFP peak (Figs. 9*A*, right, and 10*A*, top). UP states in these cells often emerged from an already relatively depolarized baseline and were not usually associated with overt membrane potential bimodality (Fig. 10*A*, top right), as is also sometimes the case for RS cells recorded *in vivo* (e.g., Fig. 1A_2) (see also Crunelli et al., 2012). However, steady hyperpolarization of these neurons via negative d.c. current injection brought about conventional-looking UP states that were associated with membrane potential bimodality (Fig. 10*A*, middle). For "early firing" neurons, action potential output occurred at a mean phase (μ) of −43.1 ± 15.5° ($n = 6$) relative to LFP oscillations with cells showing a normalized vector length (r) of 0.51 ± 0.08 ($n = 6$) (Fig. 9*B*).

Although all "early firing" cells were found to be layer 5 RS pyramidal cells, not all layer 5 RS pyramidal neurons were "early firing" cells with a substantial proportion of RS neurons (32 of 86;

←

(*Figure legend continued.*) cycles in a seemingly random fashion. ***C***, Properties of UP states in L2/3 and L5 from the recording illustrated in ***B***. Three cycles are illustrated for both supragranular and infragranular origin for three isolated single units in L5 (left, red) and L2/3 (right, blue). UP states in L5 have a higher firing rate than in L2/3 regardless of site of origin (bottom plots, left and right), but the UP states recorded in L2/3 are more prolonged when the activity originates in L2/3 (top right plot) (red arrows). $^{**}p < 0.05$.

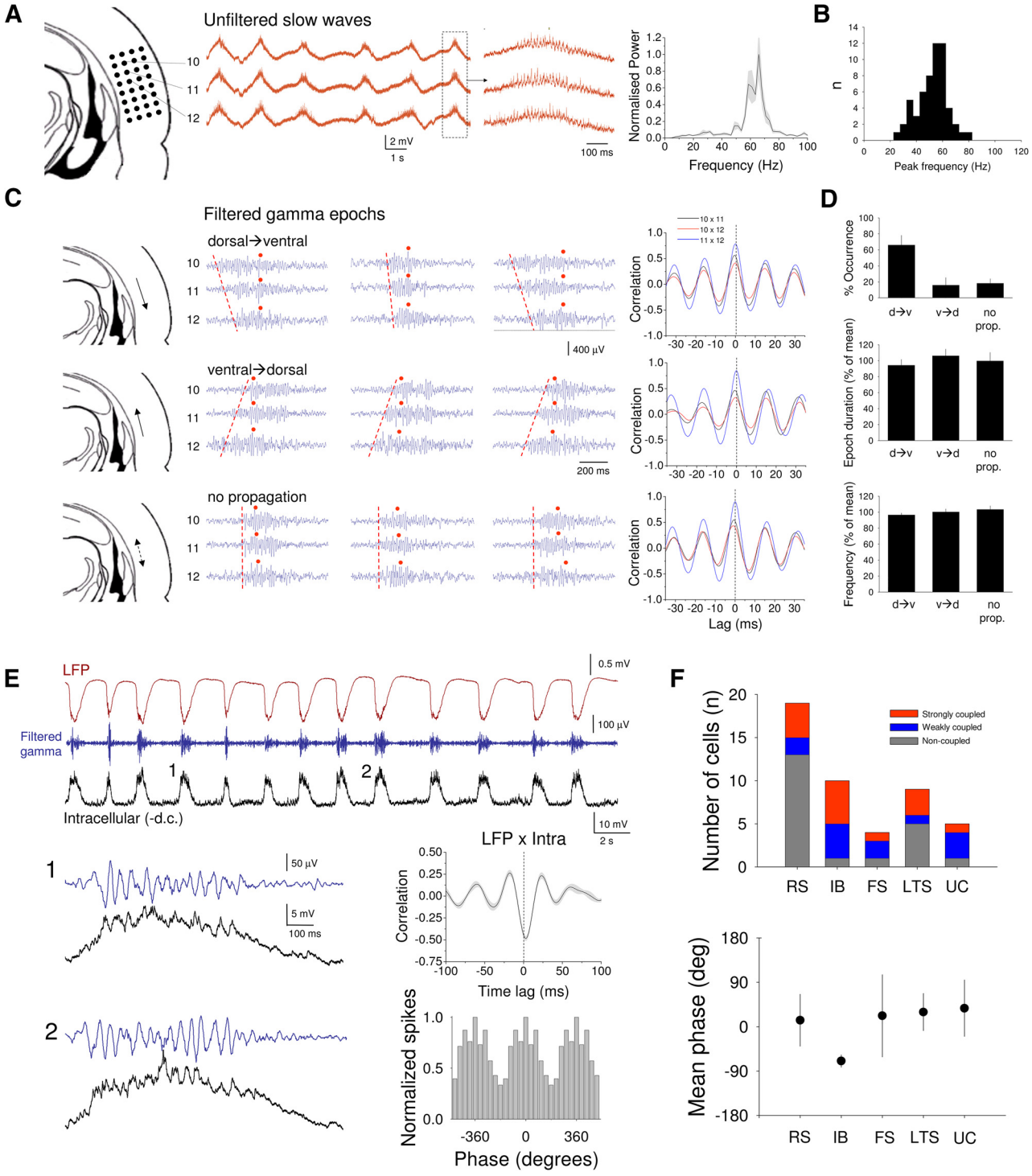

Figure 5. High-frequency (~20–100 Hz) oscillations during UP states in mouse neocortical slices. ***A***, Recording of CCH-induced LFP slow waves from 3 adjacent sites in layer 5 of the mouse auditory cortex slice (configuration shown on the left). Boxed section is expanded to the right and shows the presence of high-frequency oscillations during the UP states of the slow oscillation. Far right plot, The average power spectrum for 20 consecutive UP states. ***B***, Histogram summarizing the distribution of frequencies for high-frequency oscillations in mouse cortical slices. ***C***, Individual examples from the same 3 recording sites in ***A*** (filtered between 20 and 100 Hz) showing a mixture of dorsal ⟶ ventral propagation (top), ventral ⟶ dorsal propagation (middle), or no propagation (bottom) (dashed red lines indicate the direction of propagation). Red dots indicate the peak of the underlying slow wave. The plots to the right give all possible cross-correlogram combinations for each of the three cases and show that, regardless of propagation direction, high-frequency oscillations are always tightly synchronized within epochs. ***D***, Summary for 10 different slices with equivalent recording orientations of the proportion of different propagation directions (top), epoch duration for different propagation directions (middle), and the mean frequency of high-frequency oscillations for each case (bottom). ***E***, Simultaneous recordings of the LFP and the intracellular subthreshold activity of a layer 5 RS neuron (membrane potential: −82 mV) during CCH-induced slow waves *in vitro*. Blue trace represents the LFP recording filtered between 20 and 100 Hz. UP states (1 and 2) are enlarged below and reveal a clear correlation between synaptic activity and high-frequency network oscillations. This is confirmed by the cross-correlogram shown to the top right. This correlation translates into action potential output during UP states that is also correlated with high-frequency network oscillations, as evidenced by the spike timing histogram to the bottom right. ***F***, Top, Summary of phase coupling of different cell types (RS, IB, FS, LTS, UC) to high-frequency network oscillations (strongly coupled: $r \geq 0.2$; weakly coupled: $0.15 \leq r < 0.2$; noncoupled: $r < 0.15$). Bottom, Averaged mean phase of firing relative to the LFP (μ) for different cell types (strongly and weakly coupled cells only, RS: $n = 6$, IB: $n = 6$, FS: $n = 3$, LTS: $n = 4$, UC: $n = 4$).

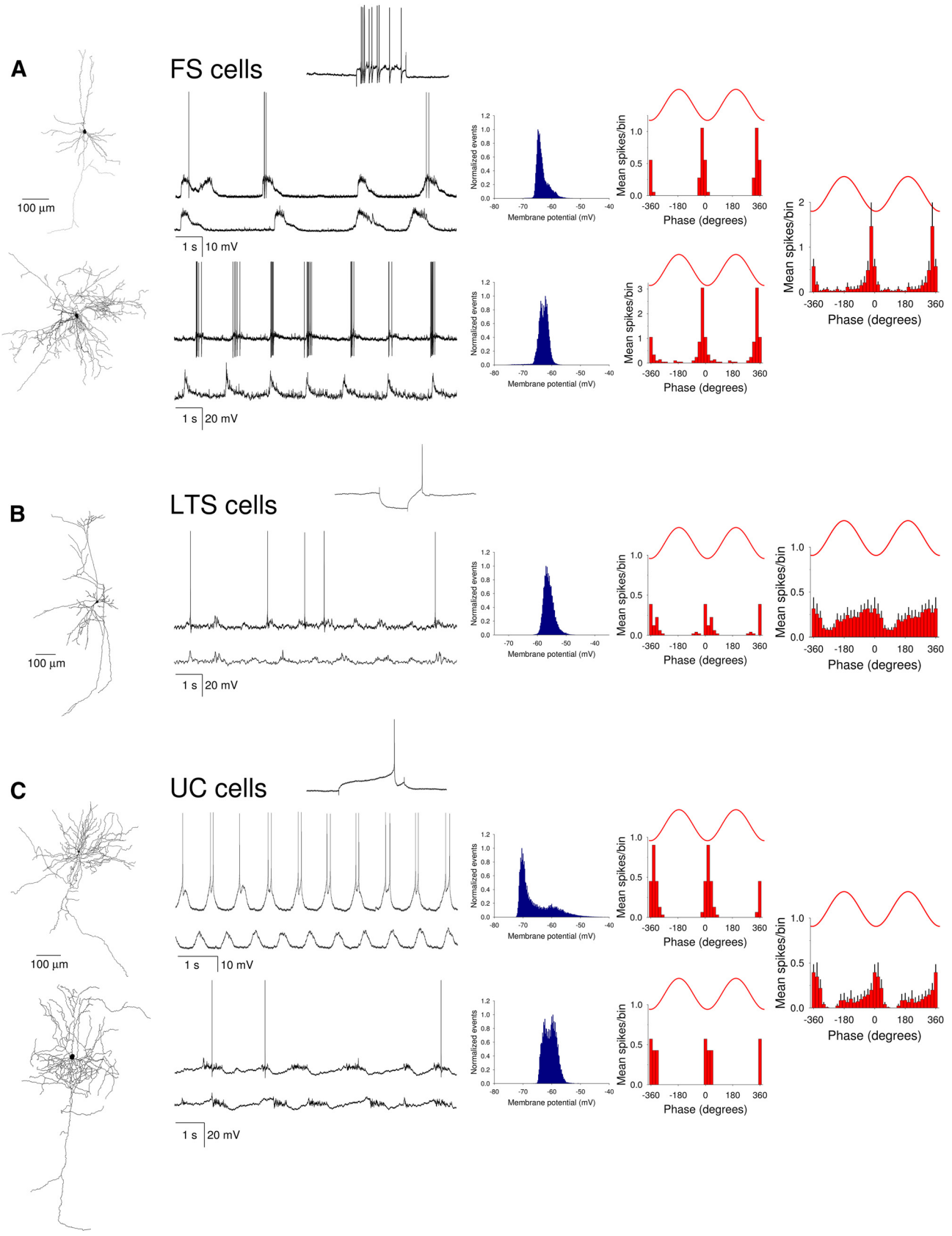

Figure 6. Characteristics of UP states in different types of nonpyramidal neurons in mouse neocortical slices. Firing properties and subthreshold membrane potential dynamics of two representative FS neurons (***A***), an LTS cell (***B***), and two UC cells (***C***). For each neuron, the reconstructed morphology is shown on the left, whereas the membrane potential distribution (blue plot) and corresponding spike timing histograms (red bars) are shown on the right. Insets, The response of the respective neurons to positive (top FS cell and top UC cell) and negative (LTS cell) current steps. Far right plots, The average spike timing histograms (mean ± SEM) for 4 FS cells, 7 LTS cells, and 5 UC cells. Most nonpyramidal cells are characterized by a lack of membrane potential bimodality and how FS cells show the strongest correlation with LFP slow waves.

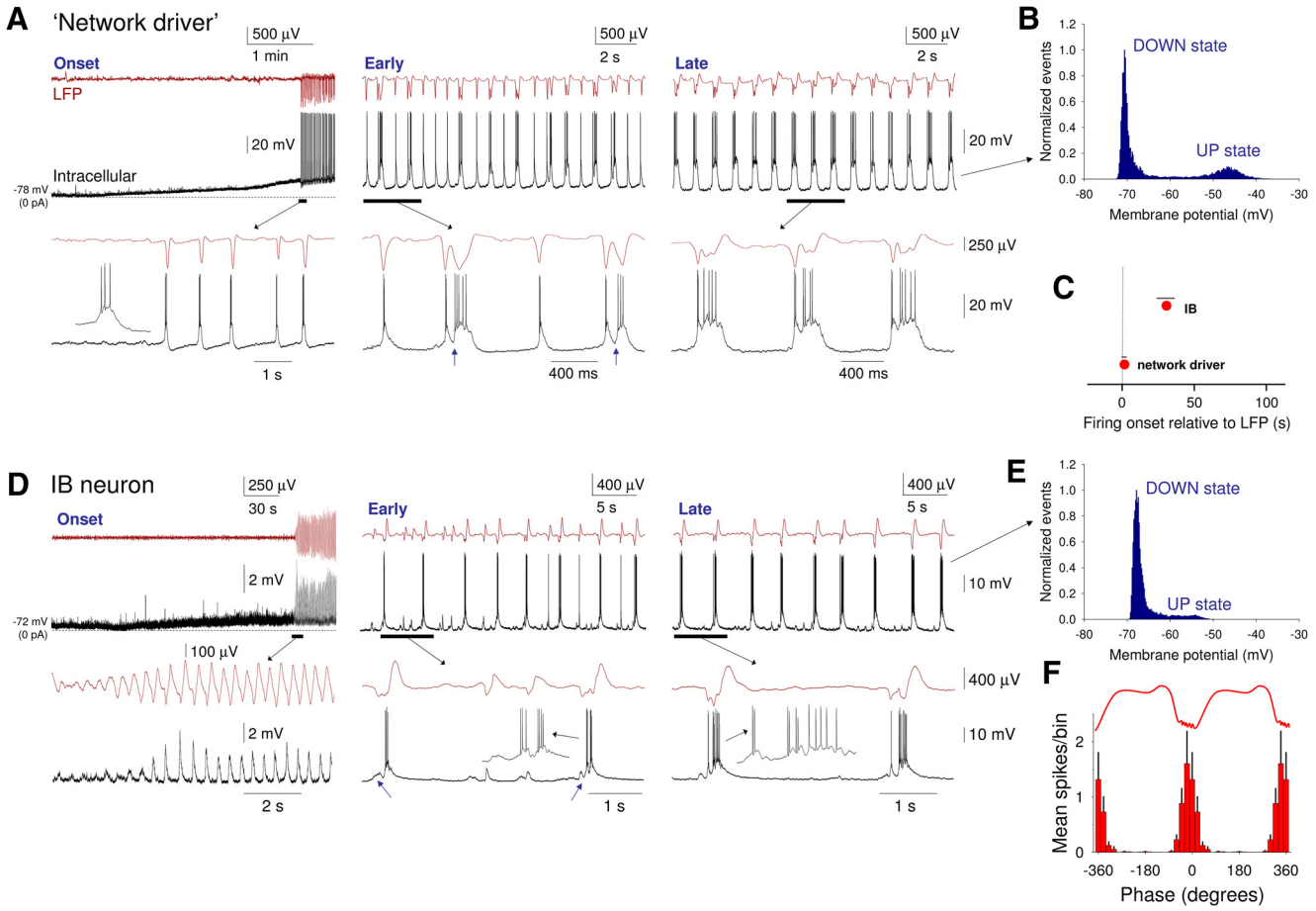

Figure 7. Comparison of the development of UP states in "network driver" cells and conventional IB neurons following cholinergic receptor activation *in vitro*. ***A***, Simultaneous recording of LFP and intracellular activity of a "network driver" neuron. Left (onset), Following bath application of CCH, the neuron is strongly depolarized and starts to exhibit rhythmic burst firing. At the same time, synchronized oscillations become evident in the LFP. The underlined section is expanded below as indicated. Inset, An individual burst. Middle (early), After a few minutes, bursts are occasionally followed by an additional depolarization indicative of recurrent excitation (see blue arrows in expanded section). Right (late), Following prolonged application of CCH, recurrent excitation occurs on every oscillation cycle leading to full-blown UP states. In all cases, UP states commence with a burst of action potentials as observed *in vivo* (e.g., Fig. 1*C*). ***B***, Plot of membrane potential distribution corresponding to the fully developed slow oscillation shown in ***A*** (late). ***C***, Quantification (mean ± SEM) of the delay between the onset of the oscillation in the LFP and onset of firing for "network driver" ($n = 6$) and conventional IB ($n = 8$) neurons. The onset of the LFP oscillation is represented at time 0. ***D***, Simultaneous recording of LFP and intracellular activity of a conventional IB neuron. Left (onset), Following bath application of CCH, the neuron is moderately depolarized and starts to exhibit rhythmic EPSP complexes in synchrony with the emergent oscillation in the LFP. The underlined section is expanded below as indicated. Middle (early), After a few minutes, EPSP complexes are occasionally crowned by burst firing. Inset in expanded section, Individual bursts. Small EPSPs (see blue arrows in expanded section) are often evident before burst generation as is the case *in vivo* (e.g., Fig. 1C_2). Right (late), Following prolonged application of CCH, action potential activity is observed on all cycles of the oscillation leading to fully developed, rhythmic UP states. Again, in all cases, UP states commence with a burst of action potentials (see inset in the expanded section). ***E***, Plot of membrane potential distribution corresponding to the fully developed slow oscillation shown in ***D*** (late). ***F***, The average spike timing histogram (mean ± SEM) computed from 14 IB neurons (combining both "network driver" and conventional IB neurons).

37%) being entrained into the oscillation through the progressive development of rhythmic EPSP complexes (Fig. 9*D*, left) that appeared following a small CCH-induced depolarization (control: −68.6 ± 5.0 mV; CCH: −64.5 ± 5.7 mV; $n = 10$). Firing in these neurons commenced after the LFP slow (<1 Hz) oscillation has been developed (delay of firing from LFP onset: 40.3 ± 7.73 s; Fig. 9*C*). In these cells once UP states were fully developed, they exhibited a conventional appearance and were associated with membrane potential bimodality (DOWN state: −67.1 ± 0.8 mV; UP state: −55.3 ± 0.6 mV; $n = 10$; Figs. 9*D*, right, and 10*B*, middle). However, steady depolarization of these neurons via positive d.c. current injection brought about UP states that were indistinguishable from those exhibited by "early firing" neurons (Fig. 10*B*, top). In non-"early firing" RS cells, action potentials occurred at a mean phase (μ) of 11.1 ± 10.9° ($n = 6$) and cells showed a normalized vector length (r) of 0.93 ± 0.02 ($n = 6$) (Fig. 9*E*). Thus, the main apparent difference between "early firing" cells and the remainder of layer 5 RS pyramidal neurons is the degree to which CCH causes a direct depolarization and spontaneous firing (Fig. 9*A*,*D*).

Blocking excitatory and inhibitory synaptic activity differentially affects UP/DOWN states in layer 5 RS and IB pyramidal neurons

In all intracellularly recorded cells in neocortical slices with added CCH, the frequency of UP states was unaltered by changes in steady injected current, further illustrating that they are dependent on network mechanisms (e.g., Fig. 10*A*,*B*). Indeed, in all neurons, hyperpolarization with steady current to prevent action potential generation revealed rhythmic barrages of synaptic activity (Fig. 10*A*,*B*, bottom traces). Consistent with these observations and further substantiating that oscillatory activity is fundamentally driven by synaptic interactions between neocortical neurons, blocking ionotropic glutamate and GABA receptors

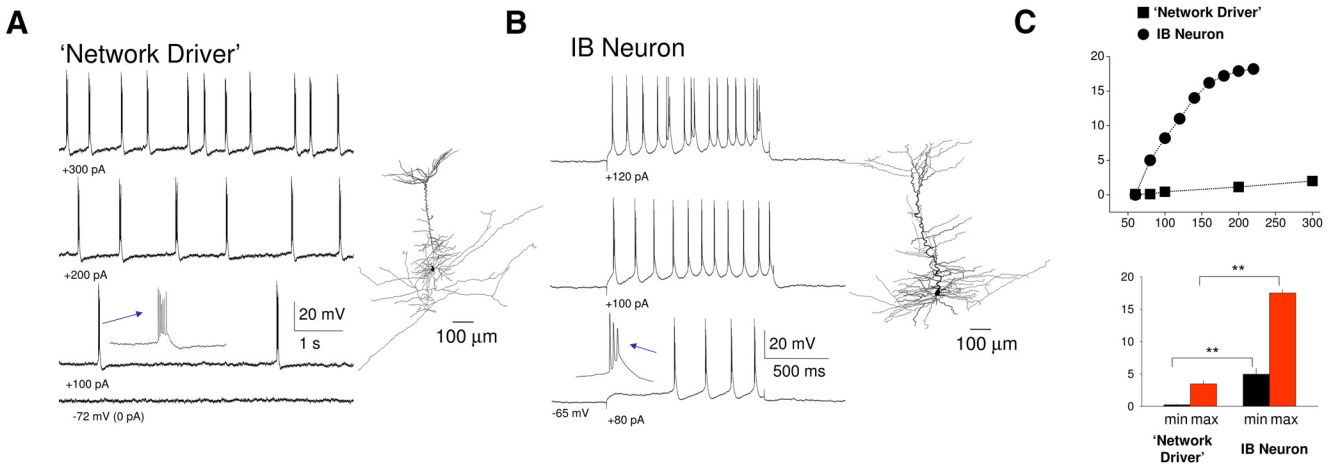

Figure 8. "Network driver" cells possess distinct intrinsic properties compared with conventional IB neurons. ***A***, In the absence of CCH, steady depolarizing current injection elicits rhythmic low-frequency bursting in a "network driver" IB neuron. Inset, A single burst. The reconstructed neuron is illustrated on the immediate right. ***B***, In the absence of CCH, depolarizing current steps elicit rhythmic bursts in a conventional IB neuron at notably higher frequencies than observed for the "network driver" neuron depicted in ***A***. The reconstructed neuron is illustrated on the immediate right. ***C***, Top, Plot showing frequency of rhythmic bursting versus injected current for the "network driver" neuron shown in ***A*** (squares) and the conventional IB neuron shown in ***B*** (circles). Bottom, Average minimum and maximum frequencies of rhythmic bursting for 6 "network driver" neurons and 8 conventional IB cells.

by applying a combination of 10 μM NBQX, 50 μM APV, 10 μM gabazine, and 10 μM CGP abolished the generation of rhythmic fluctuations in the LFP ($n = 16$ slices) (Fig. 11*A*,*B*).

Although oscillatory activity in the LFP was blocked in all cases by blocking fast excitatory and inhibitory synaptic transmission, this manipulation affected individual layer 5 pyramidal neurons in distinct ways. First, in IB neurons that were "network driver" cells, blocking synaptic transmission caused a progressive shortening of UP states until these neurons exhibited low-frequency burst firing only ($n = 4$) (Fig. 11A_1). This confirmed that the direct postsynaptic effect of CCH in these cells was to bring about intrinsic rhythmic bursting. Second, in all other IB neurons ($n = 4$) and in RS neurons, which were not "early firing" cells ($n = 4$), blocking synaptic transmission caused a gradual reduction in the amplitude of rhythmic synaptic barrages and, consequently, an abolition of action potential firing (Fig. 11A_2,B_2). Third, in "early firing" RS neurons, the pharmacological blockade of excitatory synaptic transmission led to the progressive loss of DOWN states and the appearance of continuous firing (7.6 ± 3.6 Hz; $n = 4$; Fig. 11B_1), thereby removing network input to these cells while leaving the strong, direct muscarinic depolarization intact.

Absence of rhythmic burst firing in "network driver" neurons recorded in slices maintained in a reduced extracellular Ca^{2+} concentration

In earlier studies, UP and DOWN states have been brought about in neocortical slices by modifying the ionic composition of the recording medium to supposedly more closely mimic that present *in vivo* (Sanchez-Vives and McCormick, 2000; Cossart et al., 2003; Shu et al., 2003; Cunningham et al., 2006; Rigas and Castro-Alamancos, 2007; Compte et al., 2008; Rigas and Castro-Alamancos, 2009; Fanselow and Connors, 2010). We therefore compared the effect of such a manipulation with that achieved by applying CCH in the same slices of the mouse primary auditory cortex. Following the wash-in of modified medium (i.e., 1.2 mM, Ca^{2+}, 3.5 mM K^+, 1 Mg^{2+}), we observed synchronized UP states that occurred sporadically (UP states per minute: 1.7 ± 0.4; $n = 10$), were therefore separated by very long DOWN states (27.3 ± 6.3 s; $n = 5$), and were nonrhythmic (Fig. 12*A*,*B*,*D*, left traces). On the other hand, in the same slices, a 30 min washout of this modified medium with a conventional medium (i.e., 2 mM Ca^{2+}, 3.15 mM K^+, 1 Mg^{2+}) followed by the addition of CCH brought about robust, rhythmic UP states (0.75 ± 0.12 Hz; $n = 5$) separated by DOWN states with a significantly shorter duration (0.84 ± 0.14 s; $n = 5$; $p < 0.001$) (Fig. 12*A*,*B*,*D*, right traces). Apart from an obvious difference in frequency and rhythmicity, UP states brought about by CCH application were of shorter duration (modified medium: 0.375 ± 0.07 s, CCH: 0.251 ± 0.02 s; $n = 5$; $p < 0.001$) and exhibited less firing (action potentials/UP state: modified medium: 5.4 ± 5.6 s, CCH: 3.8 ± 3 s; $n = 5$; $p < 0.05$) than those elicited by a modified recording medium (Fig. 12*A*,*C*). Otherwise, there were no obvious differences between individual UP states in the two conditions as assessed with intracellular recordings (Fig. 12*B*,*C*, enlarged traces). CCH increased the frequency of UP states following its application directly in the modified medium (UP states per minute: modified medium: 4.0 ± 2.2; modified medium + CCH: 21.3 ± 5.7, $p < 0.001$, $n = 5$, data not shown).

While performing this particular series of experiments, we obtained intracellular recordings from 3 "network driver" cells (Fig. 12*D*). As already described above, the onset of LFP oscillations following CCH application coincided exactly with rhythmic burst firing in these cells (Fig. 12*D*, right). Interestingly, however, such rhythmic burst firing never occurred in these cells in the presence of a modified recording medium (Fig. 12*D*, left).

Discussion

By using a pharmacological reinstatement of the cholinergic drive in mouse neocortical slices, which brings about rhythmic UP/DOWN states with characteristics indistinguishable from those observed *in vivo*, the main finding of this study is that neocortical UP states are fundamentally reliant on a small (~7%) subset of layer 5 IB pyramidal neurons (which we call putative "network drivers") that exhibit intrinsic burst firing at low frequencies (~0.2–2 Hz). These bursts are resistant to the block of excitatory and inhibitory transmission and occur rhythmically, but are compromised when recording in a low Ca^{2+} medium, thus explaining why UP states are sporadic and nonrhythmic in

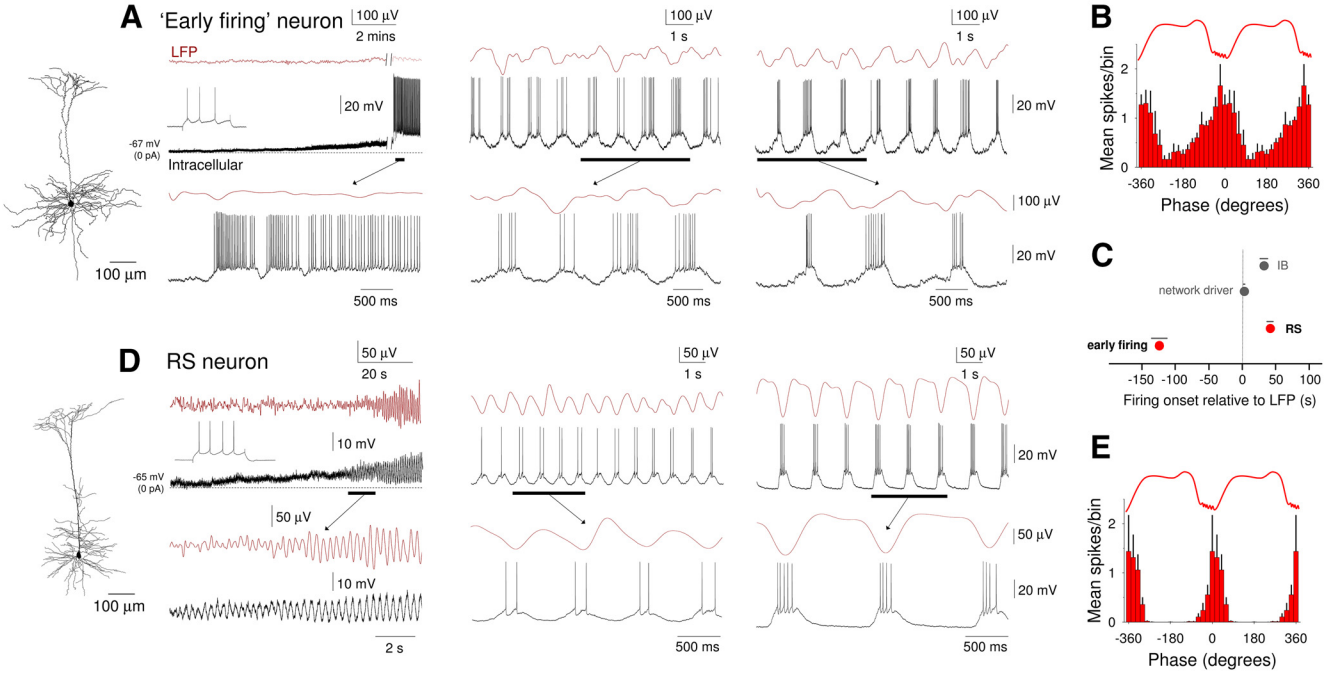

Figure 9. Comparison of the development of UP states in "early firing" and non-"early firing" RS neurons following cholinergic receptor activation. ***A***, Simultaneous recording of LFP and intracellular activity of an "early firing" neuron. Left (onset), Following bath application of CCH, the neuron is strongly depolarized and starts to exhibit continuous action potential firing. At this point, there is no oscillatory activity in the LFP. The underlined section is expanded below as indicated. Inset top, The response of this neuron to a depolarizing current step. Middle (early), After a few minutes, oscillatory activity is established in the LFP. This is gradually accompanied by the appearance of hyperpolarizing excursions in the membrane potential of the "early firing" cell. Right (late), Following prolonged application of CCH, activity in the "early firing" neuron on each oscillation cycle takes on a characteristic appearance consisting of a ramp-like depolarization and buildup of action potential firing, followed by a more abrupt hyperpolarization. The reconstructed morphology of this neuron is shown to the far left. ***B***, Average spike timing histogram (mean ± SEM) of 6 "early firing" neurons. ***C***, Quantification (mean ± SEM) of the delay between the onset of the oscillation in the LFP and onset of firing for "early firing" ($n = 11$) and non-"early firing" RS ($n = 10$) neurons; "network driver" and conventional IB neurons are also shown for comparison. ***D***, Simultaneous recording of LFP and intracellular activity of a non-"early firing" RS neuron. Left (onset), Following bath application of CCH, the neuron is moderately depolarized and starts to exhibit rhythmic EPSP complexes in synchrony with the emergent oscillation in the LFP. The underlined sections are expanded below as indicated. Inset top, The response of the neuron to a depolarizing current step. Middle (early), After a few minutes, EPSP complexes start to be crowned by one or two action potentials. Right (late), Following prolonged application of CCH, the neuron exhibits full-blown UP states with a typical step-like appearance. The reconstructed morphology of this neuron is shown to the far left. ***E***, Average spike timing histogram (mean ± SEM) of 6 non-"early firing" RS neurons.

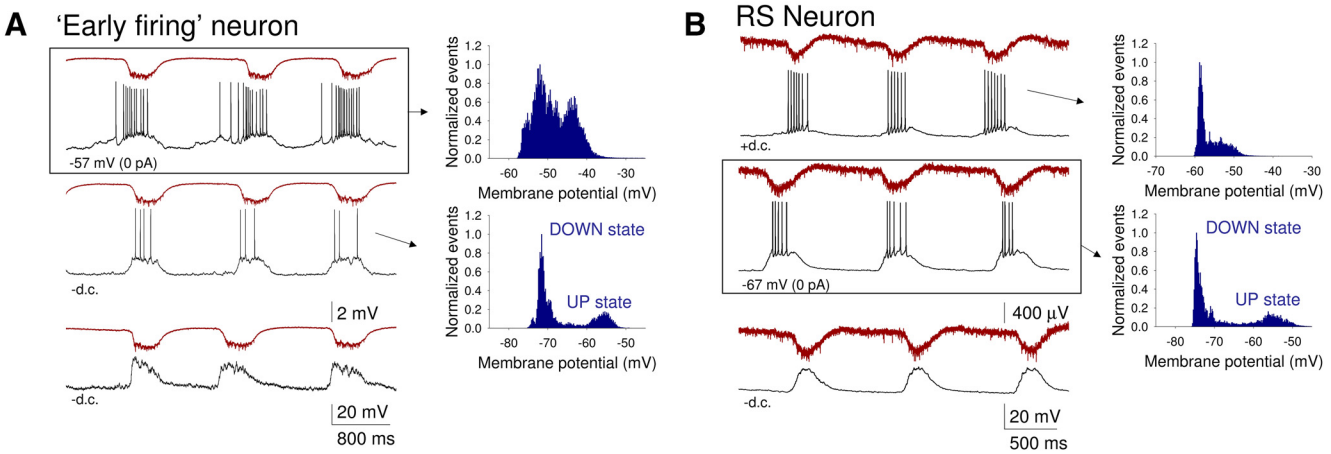

Figure 10. "Early firing" cells and other RS neurons differ only in the amount of underlying CCH-induced depolarization. ***A***, Simultaneous LFP and intracellular recording from an "early firing" RS neuron at different levels of steady injected current, as indicated, in a mouse neocortical slice. The top traces originate from a period without current injection. In this condition, the firing starts to build up before the UP state is evident in the LFP and there is a lack of membrane potential bimodality as evidenced in the plot to the immediate right. When the neuron is hyperpolarized, the firing is restricted to the UP state, which shows a more conventional step-like appearance (middle panel). In this condition, the membrane potential distribution shows clear bimodality (plot to the immediate right). Hyperpolarization below action potential firing threshold reveals the synaptic events associated with UP state generation (bottom panel). ***B***, Simultaneous LFP and intracellular recording from a non-"early firing" RS neuron at different levels of steady injected current (as indicated). The middle traces originate from a period without current injection. In this condition, the firing is restricted to the UP state, which shows a conventional step-like appearance, and the membrane potential distribution shows clear bimodality (plot to the immediate right). When the neuron is depolarized, UP states are initiated by a slower ramp-like depolarization (top panel) and there is a lack of membrane potential bimodality (plot to the immediate right). As in ***A***, hyperpolarization below action potential firing threshold reveals the synaptic events associated with UP state generation (bottom panel).

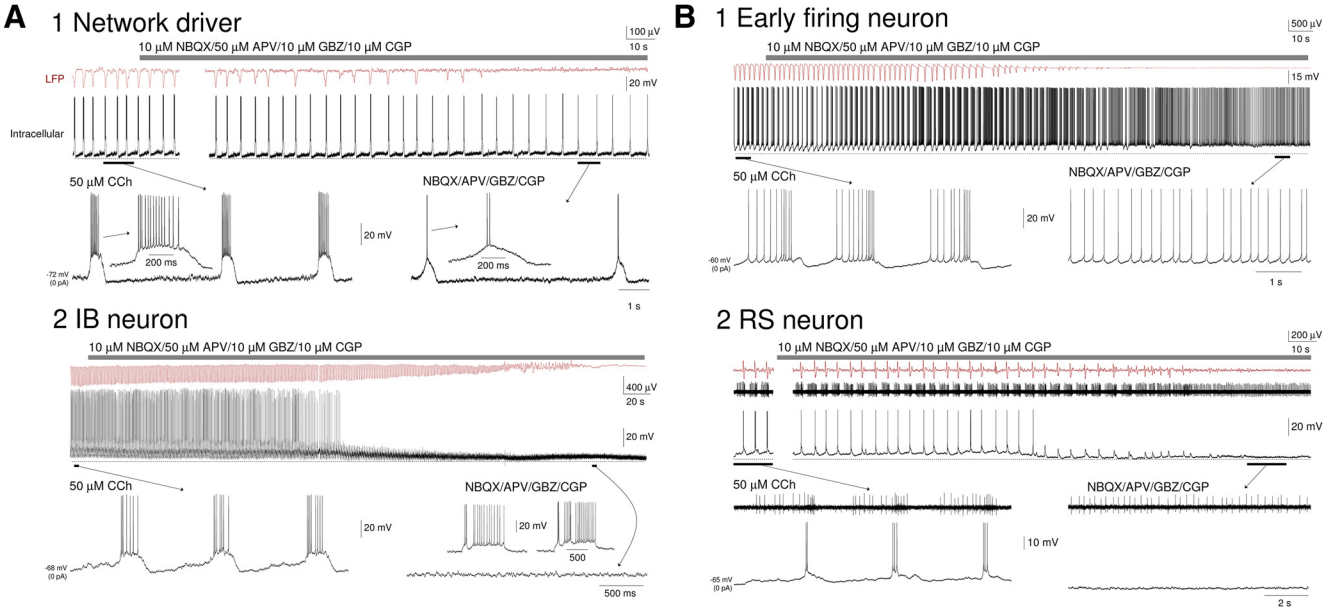

Figure 11. Blocking fast glutamatergic and GABAergic synaptic transmission differentiates "network drivers" from other IB neurons, and "early firing" cells from other RS neurons. ***A*$_1$**, Simultaneous intracellular recording of a "network driver" neuron and the proximal LFP during the slow oscillation. Blockade of fast glutamatergic and GABAergic neurotransmission (gray bar, 10 μM NBQX, 50 μM APV, 10 μM GBZ, 10 μM CGP) leads to a suppression of oscillatory activity in the LFP but leaves rhythmic burst firing in the "network driver" cell intact. In this and all subsequent panels, the underlined sections are enlarged below as indicated. ***A*$_2$**, Simultaneous intracellular recording of a conventional IB neuron and the proximal LFP during the slow oscillation. Following blockade of fast glutamatergic and GABAergic neurotransmission (gray bar, 10 μM NBQX, 50 μM APV, 10 μM GBZ, 10 μM CGP), the neuron undergoes a hyperpolarization resulting in cessation of action potential firing. Synaptic activity then gradually diminishes in parallel with a suppression of oscillatory activity in the LFP. ***B*$_1$**, Simultaneous intracellular recording of an "early firing" neuron and the proximal LFP during the slow oscillation. Following blockade of fast glutamatergic and GABAergic neurotransmission (gray bar, 10 μM NBQX, 50 μM APV, 10 μM GBZ, 10 μM CGP), there is a gradual loss of brief hyperpolarizations until the neuron displays continuous firing. This is paralleled by a gradual suppression of oscillatory activity in the LFP. ***B*$_2$**, Simultaneous recordings of the intracellular activity of a non-"early firing" RS neuron, unit activity of an "early firing" RS neuron and the proximal LFP during the slow oscillation. Following blockade of fast glutamatergic and GABAergic neurotransmission (gray bar, 10 μM NBQX, 50 μM APV, 10 μM GBZ, 10 μM CGP), there is a gradual reduction in synaptic activity and loss of firing in the non-"early firing" RS neuron that is accompanied by a loss of slow waves in the LFP. In contrast, the "early firing" neuron adopts a pattern of continuous firing as in ***B*$_1$**.

the latter experimental condition and thus different from the dynamics of the slow oscillation recorded *in vivo*.

Role of ACh in slow waves

Both the current study in mice and previous work in cats (Steriade et al., 1993b) support a role for mAChRs in shaping UP states because the systemic application of scopolamine in both species causes a pronounced reduction in UP state duration and intensity accompanied by an increase in frequency (from ~0.3 to 0.6–0.7 Hz). A recent study has shown that ACh can depolarize layer 5 pyramidal neurons and affect the UP and DOWN states present *in vitro* in a dose-dependent manner (Wester and Contreras, 2013). Although an involvement of the cholinergic system in UP state generation may seem counterintuitive, it is fully consistent with previous studies showing that during anesthesia cholinergic neurons fire prominently and preferentially during the UP state of the slow oscillation (Nunez, 1996; Détári et al., 1997; Manns et al., 2000; Mena-Segovia et al., 2008). This fits well with our finding that persistent activation of mAChRs in neocortical slices is sufficient to bring about rhythmic UP states and suggests that, at least during anesthesia, cortical UP states may be largely sustained by direct cholinergic input. In our slice experiments, a lower level of mAChR activation (i.e., during CCH wash-on) also brought about faster, lower amplitude activity at ~1–2 Hz, which closely matches the *in vivo* effects of scopolamine (Steriade et al., 1993b; but see also Carracedo et al., 2013). This increase in oscillation frequency also parallels the change that occurs in slow waves as sleep and anesthesia are deepened (Amzica and Steriade, 1998), a scenario that likely involves a lessening of cholinergic influence. Indeed, as the firing of cholinergic neurons is diminished but not abolished during natural NREM sleep (Steriade et al., 1990; Marrosu et al., 1995; Szymusiak et al., 2000; Vazquez and Baghdoyan, 2001; Lee et al., 2004, Lee et al., 2005; Hassani et al., 2009) and in humans there is a strong activation of cholinergic nuclei during NREM slow waves (Dang-Vu et al., 2008), the basic neocortical network mechanisms of UP state generation described here have also relevance to the UP/DOWN state dynamics of natural sleep (Steriade et al., 2001; Timofeev et al., 2001; Luczak et al., 2007).

Importance of intrinsic rhythmic burst firing of layer 5 "network driver" IB pyramidal neurons for initiating UP states

The initiation of network oscillations and associated UP states in this study was unequivocally due to the activity of the "network driver" cells for the following two reasons. First, at the point of inception of oscillations in the LFP, these neurons are the only group that fire coherently with this signal. Viewed another way, the fact that we could not detect any other neocortical cell type that fires in synchrony with the LFP fluctuations at the time point of slow-wave initiation, or even fires at all (with the exception of few "early firing" layer 5 RS pyramidal neurons, see below), means that only "network driver" cells, and the subsequent downstream activation of synaptic currents in neurons to which they project, can explain the LFP signal. Second, in a modified recording medium containing a reduced Ca^{2+} concentration, the intrinsic low-frequency bursting activity of "network driver" neurons that characterizes the initial response of these cells to CCH does not occur and, as a consequence, UP states are irregular and sporadic. Thus, by defining a subset of layer 5 "network driver"

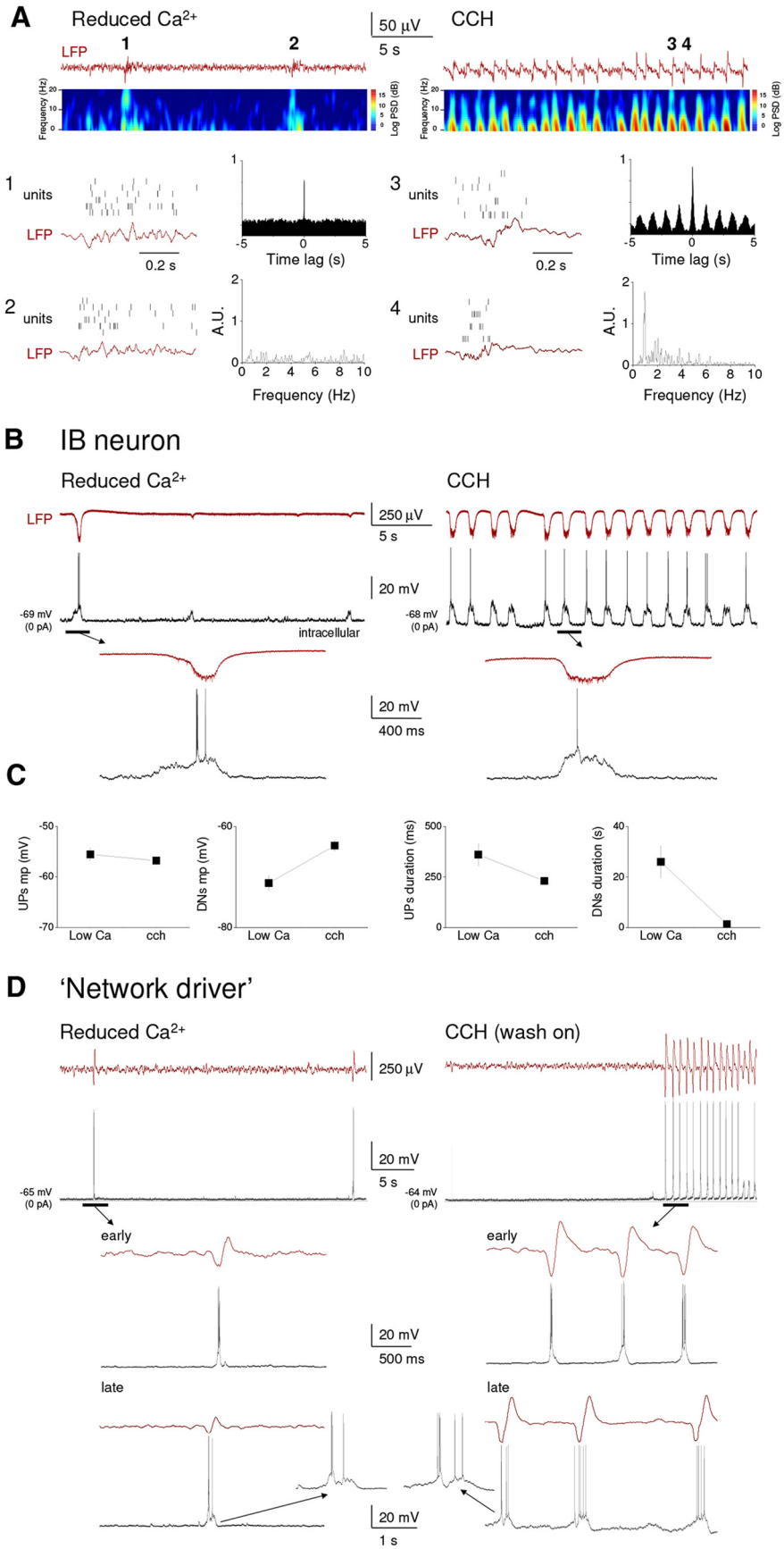

Figure 12. "Network driver" IB neurons respond differently to a reduced extracellular Ca^{2+} concentration and CCH application. ***A***, Top left, LFP recording from layer 5 of an auditory cortex slice preparation bathed in recording medium with modified ionic content (1 mM Ca^{2+}, 1 mM Mg^{2+}, 3.5 mM K^{+}; see Materials and Methods) shows sporadic, nonrhythmic activity (see cross-correlogram and FFT to the bottom left). Top right, Following wash-in of a traditional recording medium (2 mM Ca^{2+}, 1 mM Mg^{2+}, 3.25 mM K^{+}) followed in turn by the addition of CCH (30 μM) rhythmic activity becomes apparent. Corresponding spectrograms are shown immediately below the LFP traces. For each condition, two cycles of the oscillation are expanded further below (as indicated), also show simultaneously recorded unit activity. ***B***, Simultaneous recordings of the intracellular activity of a conventional layer 5 IB neurons and proximal LFP during network activity induced by either modified recording medium (left) or by adding CCH to a traditional recording medium (right). The underlined sections are expanded below as indicated. Although UP states are qualitatively similar, they display an obvious rhythmicity in the presence of CCH, which is absent in the modified recording medium. ***C***, Plots showing a summary of the differences in UP state properties between the modified recording medium and CCH conditions for 5 neurons. ***D***, Simultaneous recordings of the intracellular activity of a layer 5 "network driver" neuron and proximal LFP during the onset of network activity induced by either a modified recording medium (left) or by adding CCH to a traditional medium (right). The underlined sections are expanded below as indicated (i.e., "early" and "late"). Only following CCH application does this neuron exhibit rhythmic bursting. Hence, rhythmic network activity is only observed in this condition. This remains the case following a prolonged exposure to either condition (>15 min) as shown below ("late"). Insets, The similar nature of UP states in the two contexts.

neurons as having a key role in slow-wave generation and UP state initiation, our work provides a firm mechanistic basis for understanding the centrality of layer 5 in generating slow waves in the neocortex as previously proposed (Amzica and Steriade, 1998; Sanchez-Vives and McCormick, 2000; Sakata and Harris, 2009; Chauvette et al., 2010; Wester and Contreras, 2012; Beltramo et al., 2013).

Additional significance of cell type-specific features

Once the slow (<1 Hz) oscillation is fully established, it is likely that additional mechanisms also contribute to shaping and sustaining UP states. First, given the similarity in UP state manifestations to "network driver" neurons, it is probable that conventional IB cells (i.e., those later entrained to network activity) also play a role in driving UP states. Indeed, once network wide synchrony is established, a combined assessment of "network driver" neurons and conventional IB cells indicates that these cells (1) exhibit the strongest phase coupling to the LFP of any cell class, (2) show a peak in firing that occurs before other excitatory neurons, and (3) demonstrate UP states that nearly always commence with a burst that is subse-

quently followed by activity that is indicative of recurrent excitation.

Second, given that action potential output in "early firing" cells commences considerably before that in IB cells on each oscillation cycle, we suggest that resultant synaptic input to IB cells, and of course to other RS cells, will assist the generation of a burst, thereby facilitating full network activation. Indeed, examination of the subthreshold activity of IB neurons clearly shows the presence of EPSPs before burst generation and UP states, a feature that is also present *in vivo* (Chauvette et al., 2010). The strong tonic drive to "early firing" cells and their related activity is also consistent with several modeling studies showing that a group of neurons that are relatively depolarized, and therefore exhibit spontaneous activity, and/or the presence of spontaneous EPSPs is required to successfully simulate slow-wave activity (Bazhenov et al., 2002; Compte et al., 2003; Hill and Tononi, 2005).

Functional implications

As previously argued (Crunelli and Hughes, 2010) and recently demonstrated (David et al., 2013; Lemieux et al., 2014), the full expression of slow waves in the mammalian EEG, and in particular the robust and regular initiation of neocortical UP states, requires rhythmic input from intrinsically oscillating thalamocortical (TC) neurons. We also suggested that intrinsically rhythmic cells in the neocortex (Le Bon-Jego and Yuste, 2007) may also aid in the generation of UP states (Crunelli and Hughes, 2010). Regardless of the actual sources of pacemaker activity, the current study verifies the general concept that regularly occurring, rhythmic neocortical UP states require pacemaker input, with this pacemaker input being most effectively served by neurons, which exhibit intrinsic, rhythmic burst firing, a common feature of both TC neurons and "network driver" cells. Interestingly, that the expression of rhythmic burst firing in "network driver" cells occurs at relatively hyperpolarized membrane potentials and is replaced by tonic firing when these cells are depolarized further aligns their electrical phenotype with that of TC neurons while distinguishing them from other IB pyramidal cells in layer 5, which tend to exhibit bursting in response to stronger depolarization (Schwindt et al., 1997).

Last, given the close similarity between rhythmic network UP states that are observed during periods of reduced vigilance, such as non-REM sleep and anesthesia, and the discrete responses of the neocortex to certain types of external stimuli (Sakata and Harris, 2009), it is likely that these responses also have relevance to the processing of sensory input and for understanding fundamental neocortical circuit operations (Haider and McCormick, 2009). As such, the capacity to easily instate rhythmic UP/DOWN states in neocortical slices, as described here, may prove to be a useful tool for interrogating not only the basic mechanisms of sleep- and anesthesia-related oscillations but also the elemental structure of neocortical network dynamics during attentive states.

References

Amzica F, Steriade M (1998) Cellular substrates and laminar profile of sleep K-complex. Neuroscience 82:671–686. CrossRef Medline

Bazhenov M, Timofeev I, Steriade M, Sejnowski TJ (2002) Model of thalamocortical slow-wave sleep oscillations and transitions to activated States. J Neurosci 22:8691–8704. Medline

Beltramo R, D'Urso G, Dal Maschio M, Farisello P, Bovetti S, Clovis Y, Lassi G, Tucci V, De Pietri Tonelli D, Fellin T (2013) Layer-specific excitatory circuits differentially control recurrent network dynamics in the neocortex. Nat Neurosci 16:227–234. CrossRef Medline

Carracedo LM, Kjeldsen H, Cunnington L, Jenkins A, Schofield I, Cunningham MO, Davies CH, Traub RD, Whittington MA (2013) A neocortical δrhythm facilitates reciprocal interlaminar interactions via nested theta rhythms. J Neurosci 33:10750–10761. CrossRef Medline

Chagnac-Amitai Y, Luhmann HJ, Prince DA (1990) Burst generating and regular spiking layer 5 pyramidal neurons of rat neocortex have different morphological features. J Comp Neurol 296:598–613. CrossRef Medline

Chauvette S, Volgushev M, Timofeev I (2010) Origin of active states in local neocortical networks during slow sleep oscillation. Cereb Cortex 20:2660–2674. CrossRef Medline

Compte A, Sanchez-Vives MV, McCormick DA, Wang XJ (2003) Cellular and network mechanisms of slow oscillatory activity (<1 Hz) and wave propagations in a cortical network model. J Neurophysiol 89:2707–2725. CrossRef Medline

Compte A, Reig R, Descalzo VF, Harvey MA, Puccini GD, Sanchez-Vives MV (2008) Spontaneous high-frequency (10–80 Hz) oscillations during up states in the cerebral cortex in vitro. J Neurosci 28:13828–13844. CrossRef Medline

Cossart R, Aronov D, Yuste R (2003) Attractor dynamics of network UP states in the neocortex. Nature 423:283–288. CrossRef Medline

Crunelli V, Hughes SW (2010) The slow (<1 Hz) rhythm of non-REM sleep: a dialogue between three cardinal oscillators. Nat Neurosci 13:9–17. CrossRef Medline

Crunelli V, Lőrincz ML, Errington AC, Hughes SW (2012) Activity of cortical and thalamic neurons during the slow (<1 Hz) rhythm in the mouse in vivo. Pflugers Arch 463:73–88. CrossRef Medline

Cunningham MO, Pervouchine DD, Racca C, Kopell NJ, Davies CH, Jones RS, Traub RD, Whittington MA (2006) Neuronal metabolism governs cortical network response state. Proc Natl Acad Sci U S A 103:5597–5601. CrossRef Medline

Dang-Vu TT, Schabus M, Desseilles M, Albouy G, Boly M, Darsaud A, Gais S, Rauchs G, Sterpenich V, Vandewalle G, Carrier J, Moonen G, Balteau E, Degueldre C, Luxen A, Phillips C, Maquet P (2008) Spontaneous neural activity during human slow wave sleep. Proc Natl Acad Sci U S A 105:15160–15165. CrossRef Medline

David F, Schmiedt JT, Taylor HL, Orban G, Di Giovanni G, Uebele VN, Renger JJ, Lambert RC, Leresche N, Crunelli V (2013) Essential thalamic contribution to slow waves of natural sleep. J Neurosci 33:19599–19610. CrossRef Medline

Détári L, Rasmusson DD, Semba K (1997) Phasic relationship between the activity of basal forebrain neurons and cortical EEG in urethane-anesthetized rat. Brain Res 759:112–121. CrossRef Medline

Fanselow EE, Connors BW (2010) The roles of somatostatin-expressing (GIN) and fast-spiking inhibitory interneurons in UP-DOWN states of mouse neocortex. J Neurophysiol 104:596–606. CrossRef Medline

Franceschetti S, Buzio S, Sancini G, Panzica F, Avanzini G (1993) Expression of intrinsic bursting properties in neurons of maturing sensorimotor cortex. Neurosci Lett 162:25–28. CrossRef Medline

Haider B, McCormick DA (2009) Rapid neocortical dynamics: cellular and network mechanisms. Neuron 62:171–189. CrossRef Medline

Hasenstaub A, Shu Y, Haider B, Kraushaar U, Duque A, McCormick DA (2005) Inhibitory postsynaptic potentials carry synchronized frequency information in active cortical networks. Neuron 47:423–435. CrossRef Medline

Hassani OK, Lee MG, Henny P, Jones BE (2009) Discharge profiles of identified GABAergic in comparison to cholinergic and putative glutamatergic basal forebrain neurons across the sleep–wake cycle. J Neurosci 29:11828–11840. CrossRef Medline

Hill S, Tononi G (2005) Modeling sleep and wakefulness in the thalamocortical system. J Neurophysiol 93:1671–1698. CrossRef Medline

Hughes S, Crunelli V (2013) UP states rise from the depths. Nat Neurosci 16:115–117. CrossRef Medline

Le Bon-Jego M, Yuste R (2007) Persistently active, pacemaker-like neurons in neocortex. Front Neurosci 1:123–129. CrossRef Medline

Lee MG, Manns ID, Alonso A, Jones BE (2004) Sleep–wake related discharge properties of basal forebrain neurons recorded with micropipettes in head-fixed rats. J Neurophysiol 92:1182–1198. CrossRef Medline

Lee MG, Hassani OK, Alonso A, Jones BE (2005) Cholinergic basal forebrain neurons burst with theta during waking and paradoxical sleep. J Neurosci 25:4365–4369. CrossRef Medline

Lemieux M, Chen JY, Lonjers P, Bazhenov M, Timofeev I (2014) The impact of cortical deafferentation on the neocortical slow oscillation. J Neurosci 34:5689–5703. CrossRef Medline

Lőrincz ML, Kékesi KA, Juhász G, Crunelli V, Hughes SW (2009) Temporal framing of thalamic relay-mode firing by phasic inhibition during the alpha rhythm. Neuron 63:683–696. CrossRef Medline

Luczak A, Barthó P, Marguet SL, Buzsáki G, Harris KD (2007) Sequential structure of neocortical spontaneous activity in vivo. Proc Natl Acad Sci U S A 104:347–352. CrossRef Medline

Manns ID, Alonso A, Jones BE (2000) Discharge properties of juxtacellularly labeled and immunohistochemically identified cholinergic basal forebrain neurons recorded in association with the electroencephalogram in anesthetized rats. J Neurosci 20:1505–1518. Medline

Marrosu F, Portas C, Mascia MS, Casu MA, Fà M, Giagheddu M, Imperato A, Gessa GL (1995) Microdialysis measurement of cortical and hippocampal acetylcholine release during sleep–wake cycle in freely moving cats. Brain Res 671:329–332. CrossRef Medline

Mena-Segovia J, Sims HM, Magill PJ, Bolam JP (2008) Cholinergic brainstem neurons modulate cortical gamma activity during slow oscillations. J Physiol 586:2947–2960. CrossRef Medline

Mukovski M, Chauvette S, Timofeev I, Volgushev M (2007) Detection of active and silent states in neocortical neurons from the field potential signal during slow-wave sleep. Cereb Cortex 17:400–414. CrossRef Medline

Nunez A (1996) Unit activity of rat basal forebrain neurons: relationship to cortical activity. Neuroscience 72:757–766. CrossRef Medline

Rigas P, Castro-Alamancos MA (2007) Thalamocortical Up states: differential effects of intrinsic and extrinsic cortical inputs on persistent activity. J Neurosci 27:4261–4272. CrossRef Medline

Rigas P, Castro-Alamancos MA (2009) Impact of persistent cortical activity (up states) on intracortical and thalamocortical synaptic inputs. J Neurophysiol 102:119–131. CrossRef Medline

Ruiz-Mejias M, Ciria-Suarez L, Mattia M, Sanchez-Vives MV (2011) Slow and fast rhythms generated in the cerebral cortex of the anesthetized mouse. J Neurophysiol 106:2910–2921. CrossRef Medline

Sakata S, Harris KD (2009) Laminar structure of spontaneous and sensory-evoked population activity in auditory cortex. Neuron 64:404–418. CrossRef Medline

Sanchez-Vives MV, McCormick DA (2000) Cellular and network mechanisms of rhythmic recurrent activity in neocortex. Nat Neurosci 3:1027–1034. CrossRef Medline

Schwindt P, O'Brien JA, Crill W (1997) Quantitative analysis of firing properties of pyramidal neurons from layer 5 of rat sensorimotor cortex. J Neurophysiol 77:2484–2498. Medline

Shu Y, Hasenstaub A, McCormick DA (2003) Turning on and off recurrent balanced cortical activity. Nature 423:288–293. CrossRef Medline

Steriade M, Datta S, Paré D, Oakson G, Curró Dossi RC (1990) Neuronal activities in brain-stem cholinergic nuclei related to tonic activation processes in thalamocortical systems. J Neurosci 10:2541–2559. Medline

Steriade M, Nuñez A, Amzica F (1993a) Intracellular analysis of relations between the slow (<1 Hz) neocortical oscillation and other sleep rhythms of the electroencephalogram. J Neurosci 13:3266–3283. Medline

Steriade M, Amzica F, Nuñez A (1993b) Cholinergic and noradrenergic modulation of the slow (approximately 0.3 Hz) oscillation in neocortical cells. J Neurophysiol 70:1385–1400. Medline

Steriade M, Nuñez A, Amzica F (1993c) A novel slow (<1 Hz) oscillation of neocortical neurons in vivo: depolarizing and hyperpolarizing components. J Neurosci 13:3252–3265. Medline

Steriade M, Contreras D, Amzica F, Timofeev I (1996) Synchronization of fast (30–40 Hz) spontaneous oscillations in intrathalamic and thalamocortical networks. J Neurosci 16:2788–2808. Medline

Steriade M, Timofeev I, Grenier F (2001) Natural waking and sleep states: a view from inside neocortical neurons. J Neurophysiol 85:1969–1985. Medline

Szymusiak R, Alam N, McGinty D (2000) Discharge patterns of neurons in cholinergic regions of the basal forebrain during waking and sleep. Behav Brain Res 115:171–182. CrossRef Medline

Timofeev I, Chauvette S (2011) Thalamocortical oscillations: local control of EEG slow waves. Curr Top Med Chem 11:2457–2471. CrossRef Medline

Timofeev I, Grenier F, Steriade M (2001) Disfacilitation and active inhibition in the neocortex during the natural sleep–wake cycle: an intracellular study. Proc Natl Acad Sci U S A 98:1924–1929. CrossRef Medline

Vazquez J, Baghdoyan HA (2001) Basal forebrain acetylcholine release during REM sleep is significantly greater than during waking. Am J Physiol Regul Integr Comp Physiol 280:R598–R601. Medline

Wang Z, McCormick DA (1993) Control of firing mode of corticotectal and corticopontine layer V burst-generating neurons by norepinephrine, acetylcholine, and 1S,3R-ACPD. J Neurosci 13:2199–2216. Medline

Wester JC, Contreras D (2012) Columnar interactions determine horizontal propagation of recurrent network activity in neocortex. J Neurosci 32:5454–5471. CrossRef Medline

Wester JC, Contreras D (2013) Differential modulation of spontaneous and evoked thalamocortical network activity by acetylcholine level in vitro. J Neurosci 33:17951–17966. CrossRef Medline